

Support Information

Electron Beam Etching of CaO Crystals Observed Atom by Atom

*Yuting Shen[†], Tao Xu^{†,‡}, Xiaodong Tan[†], Jun Sun[†], Longbing He^{†,‡}, Kuibo Yin^{†,‡},
Yilong Zhou[†], Florian Banhart[§] & Litao Sun^{*†,‡}*

[†]SEU–FEI Nano–Pico Center, Key Lab of MEMS of Ministry of Education,
Collaborative Innovation Center for Micro/Nano Fabrication, Device and System,
Southeast University, Nanjing 210096, People’s Republic of China

[‡] Center for Advanced Materials and Manufacture, Joint Research Institute of
Southeast University and Monash University, Suzhou 215123, People’s Republic of
China

[§]Institut de Physique et Chimie des Matériaux, Université de Strasbourg, CNRS,
UMR 7504, 67034 Strasbourg, France

*Address all correspondence to this author.

e–mail: slt@seu.edu.cn

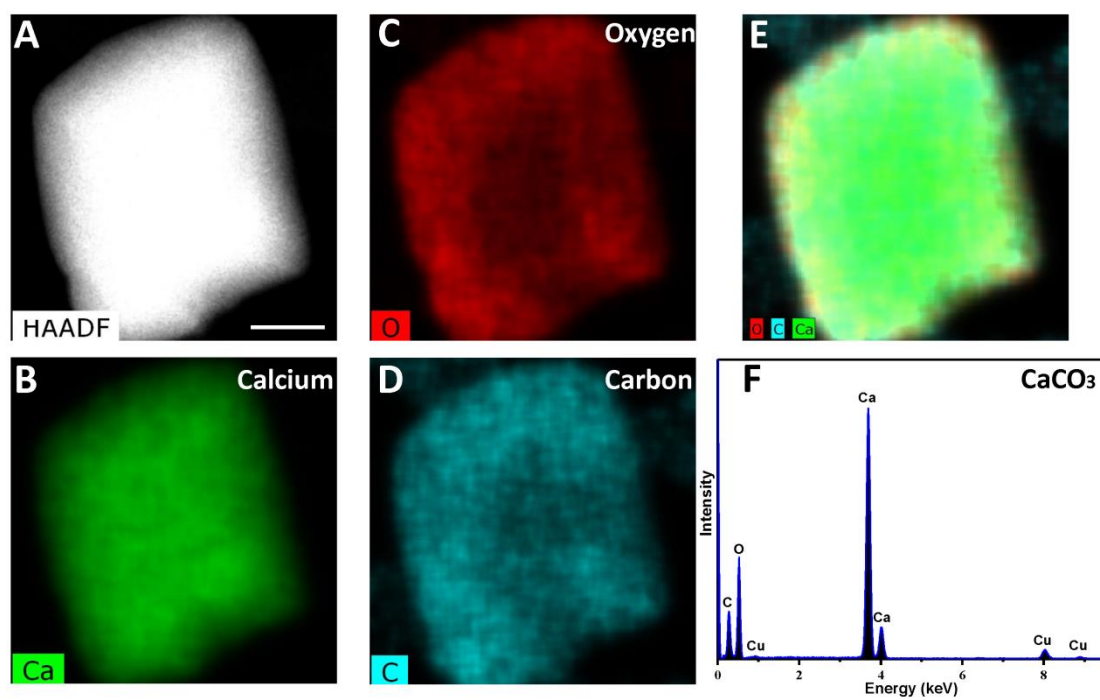


Figure S1. STEM EDS analysis of CaCO₃. (A) HAADF image of the CaCO₃ sample. (B–D) Corresponding STEM-EDS elemental mapping images for Ca (B), O (C) and C (D). (E) Integrated elemental mapping image of (B), (C) and (D). (F) The corresponding EDS spectrum. Scale bar is 1 μ m.

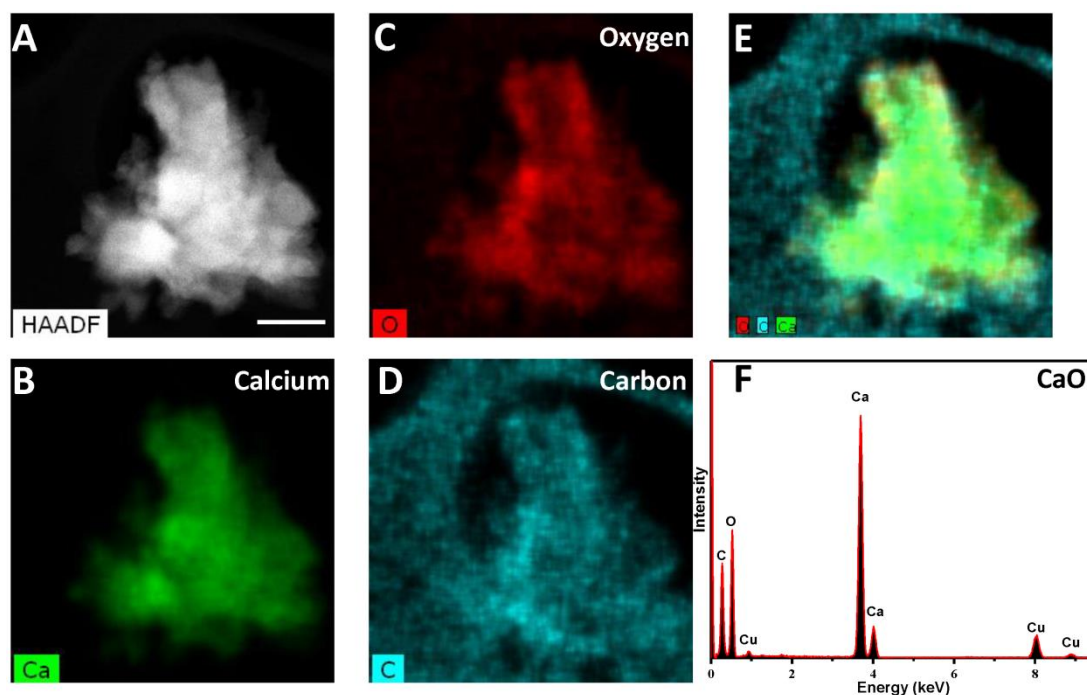


Figure S2. STEM EDS analysis of CaO. (A) HAADF image of the CaO sample. (B–D) Corresponding STEM-EDS elemental mapping images for Ca (B), O (C) and C (D). (E) Integrated elemental mapping image of (B), (C) and (D). (F) The corresponding EDS spectrum. Scale bar is 1 μm .

From the EDS mapping images in Figures S1 and S2, it can be clearly observed that the CaCO_3 and CaO samples include Ca, O and C elements. As shown in Figure S1F and S2F, there are Ca, C, O and Cu peaks in the spectra. C peaks may come from the CaCO_3 or the TEM grid, which includes both C and Cu. Cu peaks may derive from TEM grid or specimen holder. For the more precise analysis, EELS has been done to exclude the uncertainties in EDS.

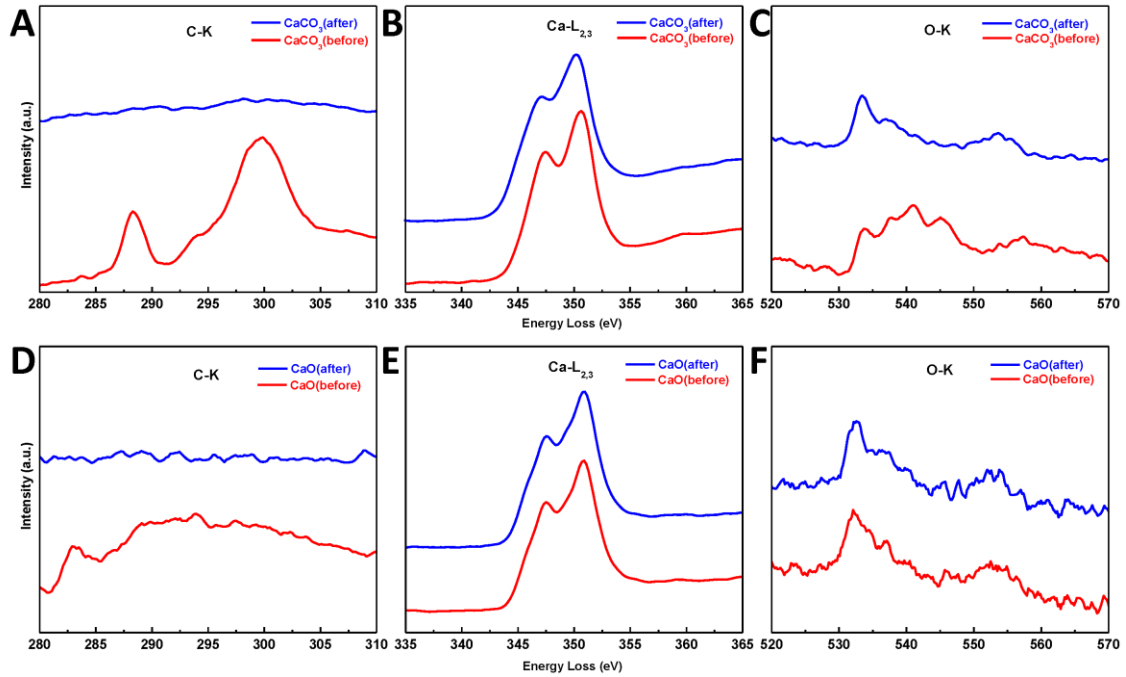


Figure S3. Electron energy-loss spectroscopy (EELS) spectra for CaCO_3 and CaO before and after electron irradiation. (A–C) C–K (A), Ca– $L_{2,3}$ (B) and O–K (C) edge of CaCO_3 , (D–F) C–K (D), Ca– $L_{2,3}$ (E) and O–K (F) edge of CaO . Red and blue lines indicate the EELS spectra before and after irradiation.

As shown in Figure S3 (A–C), the C–K and O–K peak have significant changes where the C–K peak disappears and the peak shape of O–K is different after electron beam irradiation. Before electron beam irradiation, the O–K edge is a superposition of the hybridization of oxygen with calcium and carbon (red line in Figure S3C). After electron beam irradiation, the preservation of the first peak indicates that the hybridization of the Ca atom is conserved. This can be assigned to hybridization of the oxygen $2p$ with the Ca $3d$ energy levels.¹ The second to fourth peaks are broadened or diminish, which means the hybridization with carbon is finally lost and the amount of oxygen is reduced because of the decarbonization.² The result agrees

with that of Golla-Schindler¹, thus CaCO_3 has transformed to CaO after electron beam irradiation. For the CaO in Figure S3 (D–F), there is a C–K peak before irradiation, but the shape differs from that of the CaCO_3 , which may come from the amorphous carbon impurities. After irradiation, the C–K peak disappears as well. The O–K peak has no significant change before and after irradiation.

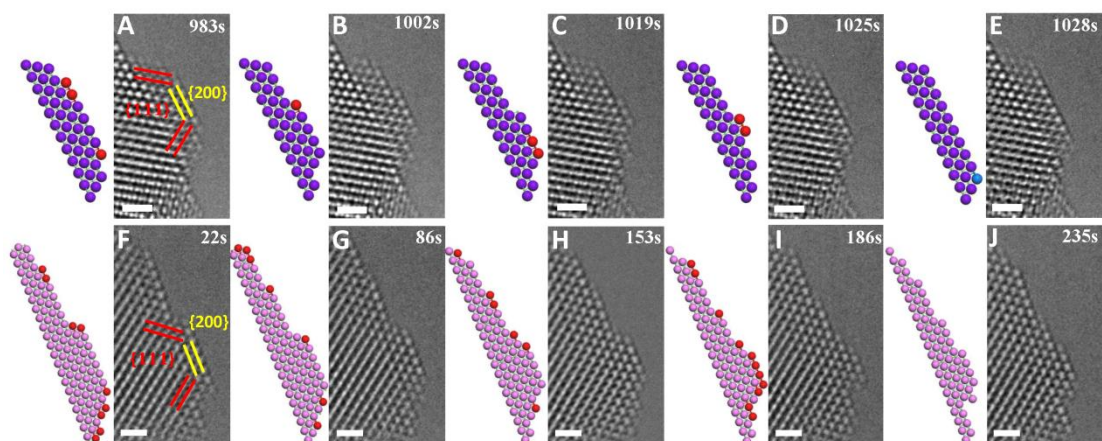
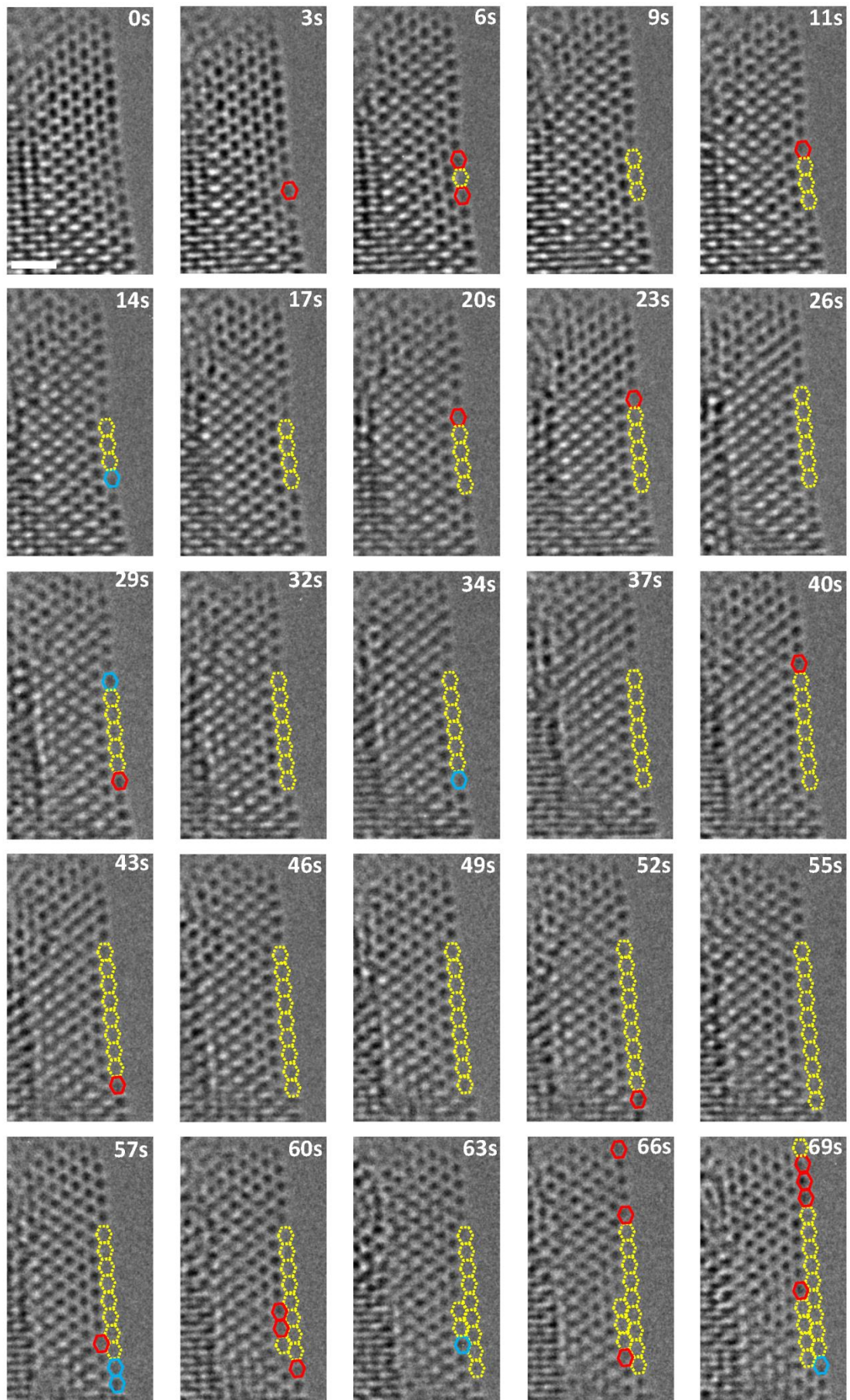


Figure S4. Representative HRTEM images illustrating the etching processes of the two different pyramidal CaO islands on the surface (A–E) and (F–J) (selected from Video 3 and 4). In order to distinguish the two etching processes, the Ca atoms were labeled by purple and pink balls in the two edges. The left side is the stick-and-ball model, and the right side is the HRTEM image. The red balls indicate those atoms that are sputtered in the next frame, whereas the dark blue balls indicate the adatoms. Scale bar is 1 nm.

The metastable atoms at the rim of the edges were gradually ejected by electron beam, and the number of the outermost layer became less and less until the whole layer disappeared (Figure S4E and S4J). Then the second layer became the new outermost layer and the etching process continued.



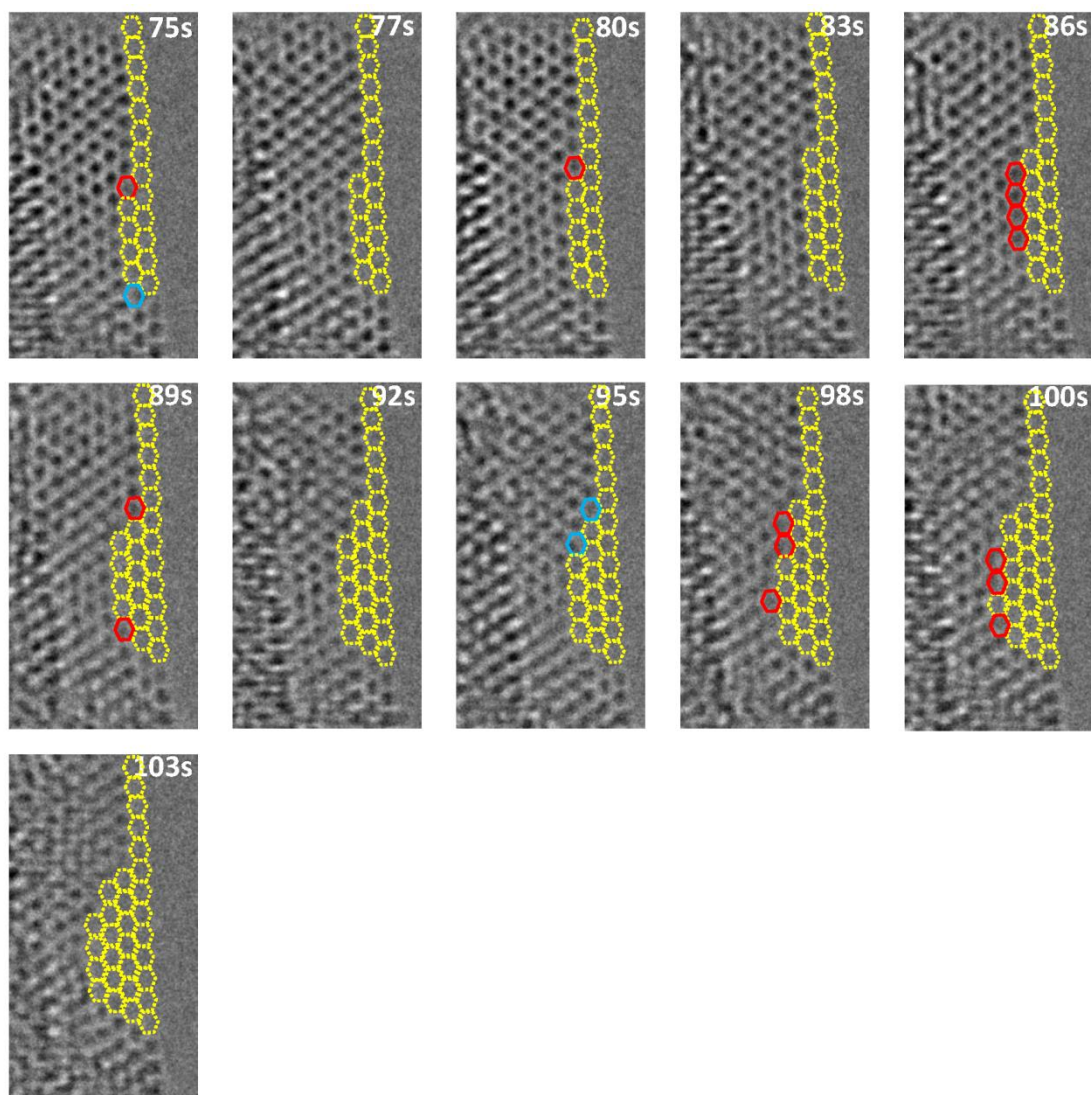
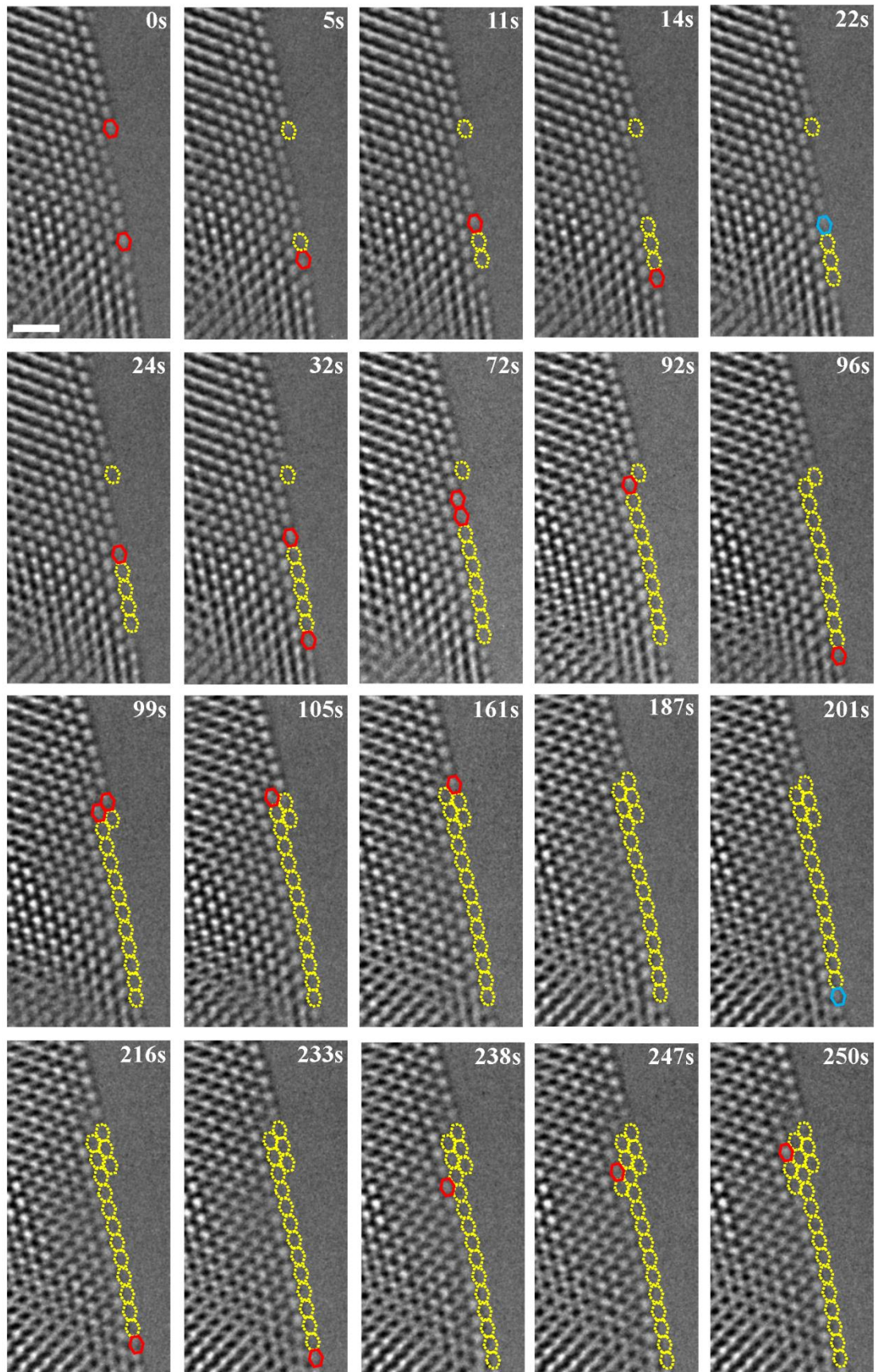
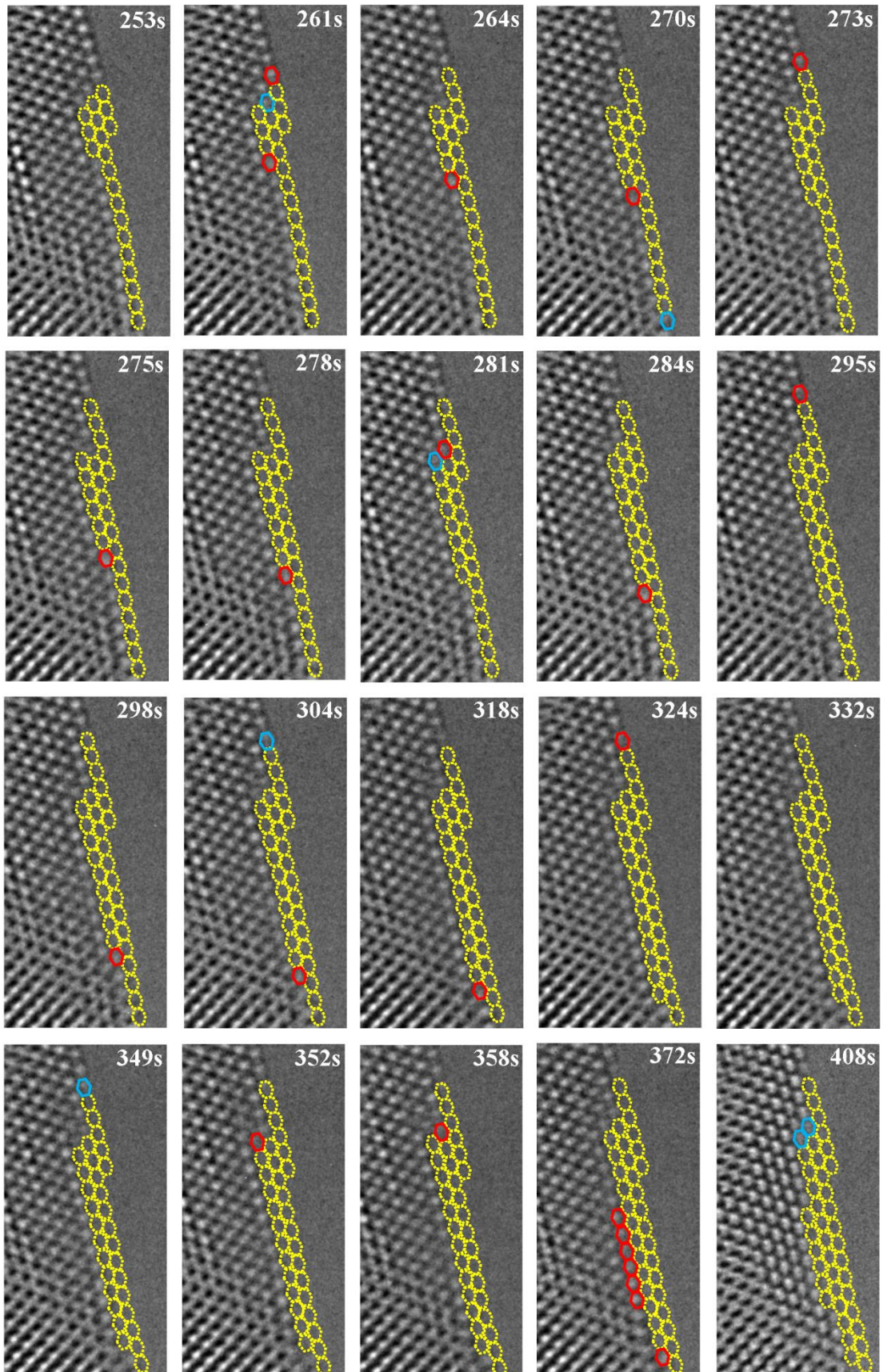
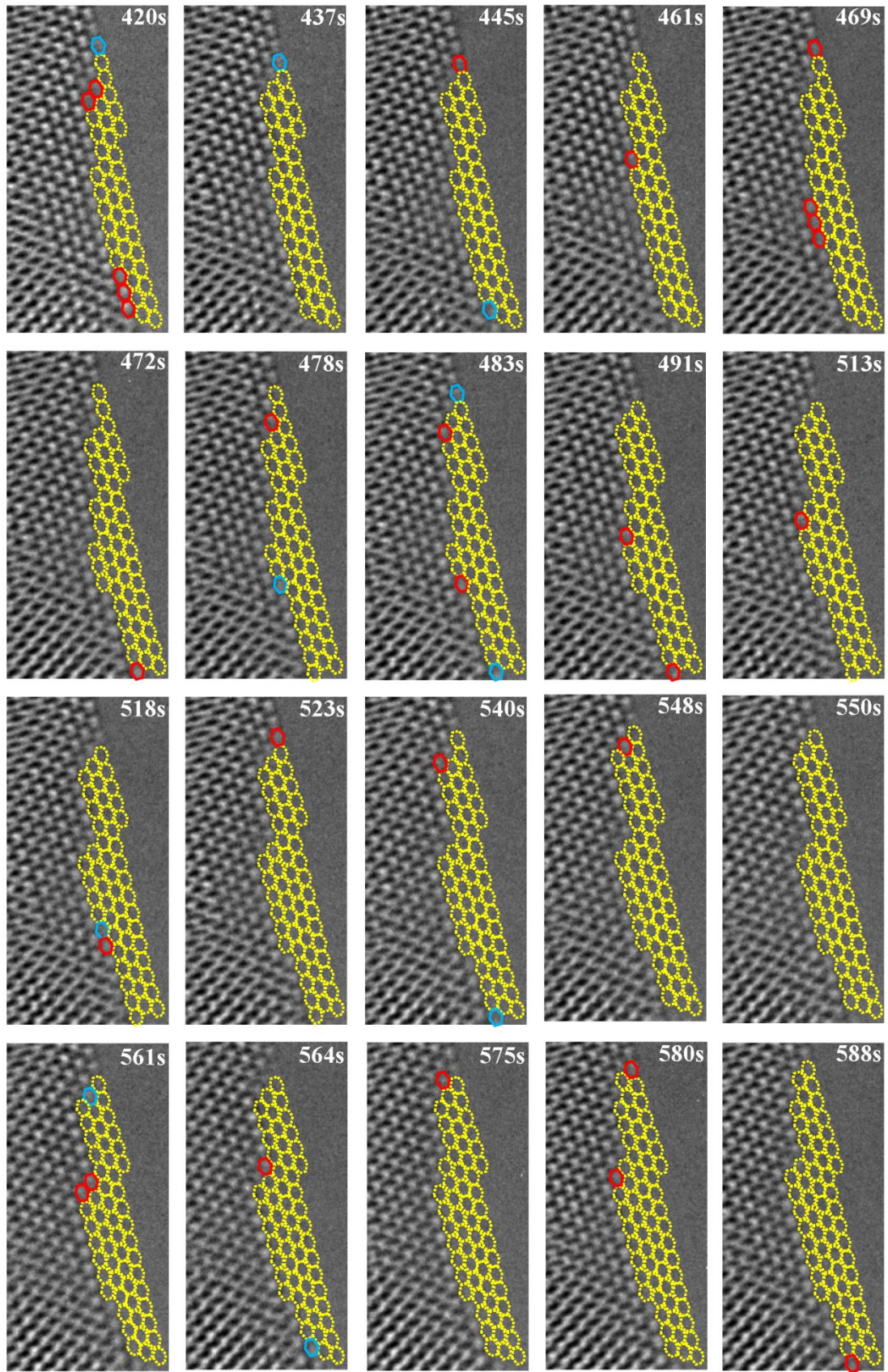
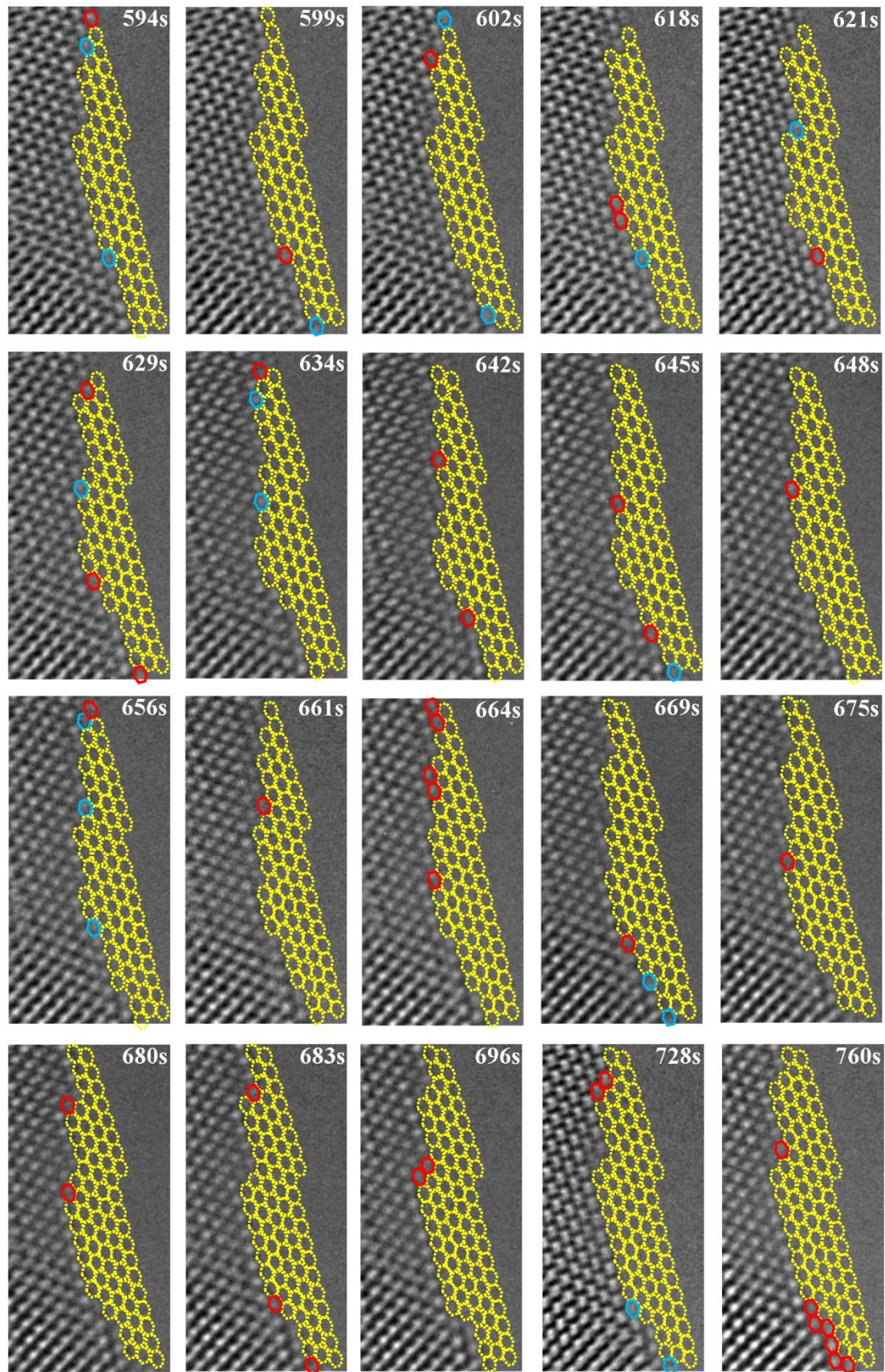


Figure S5. HRTEM image series illustrating the *in situ* electron beam etching process of the CaO surface (from Video 1). The atoms with red overlays in HRTEM images indicate that they will be sputtered in the next frame, whereas the atoms with blue overlays indicate the adatoms. The yellow overlays label the atoms that have been ejected. Scale bar is 1 nm.









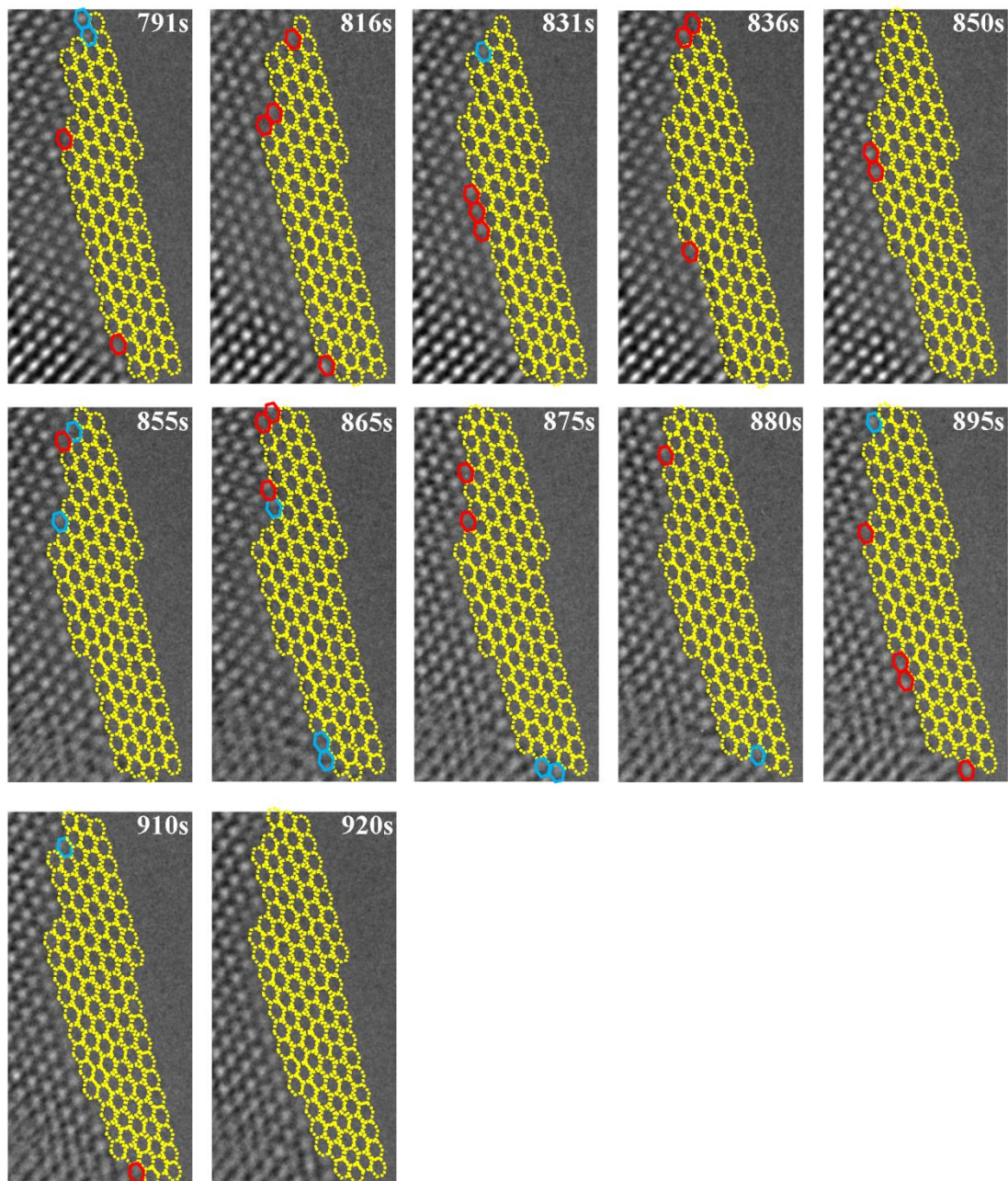
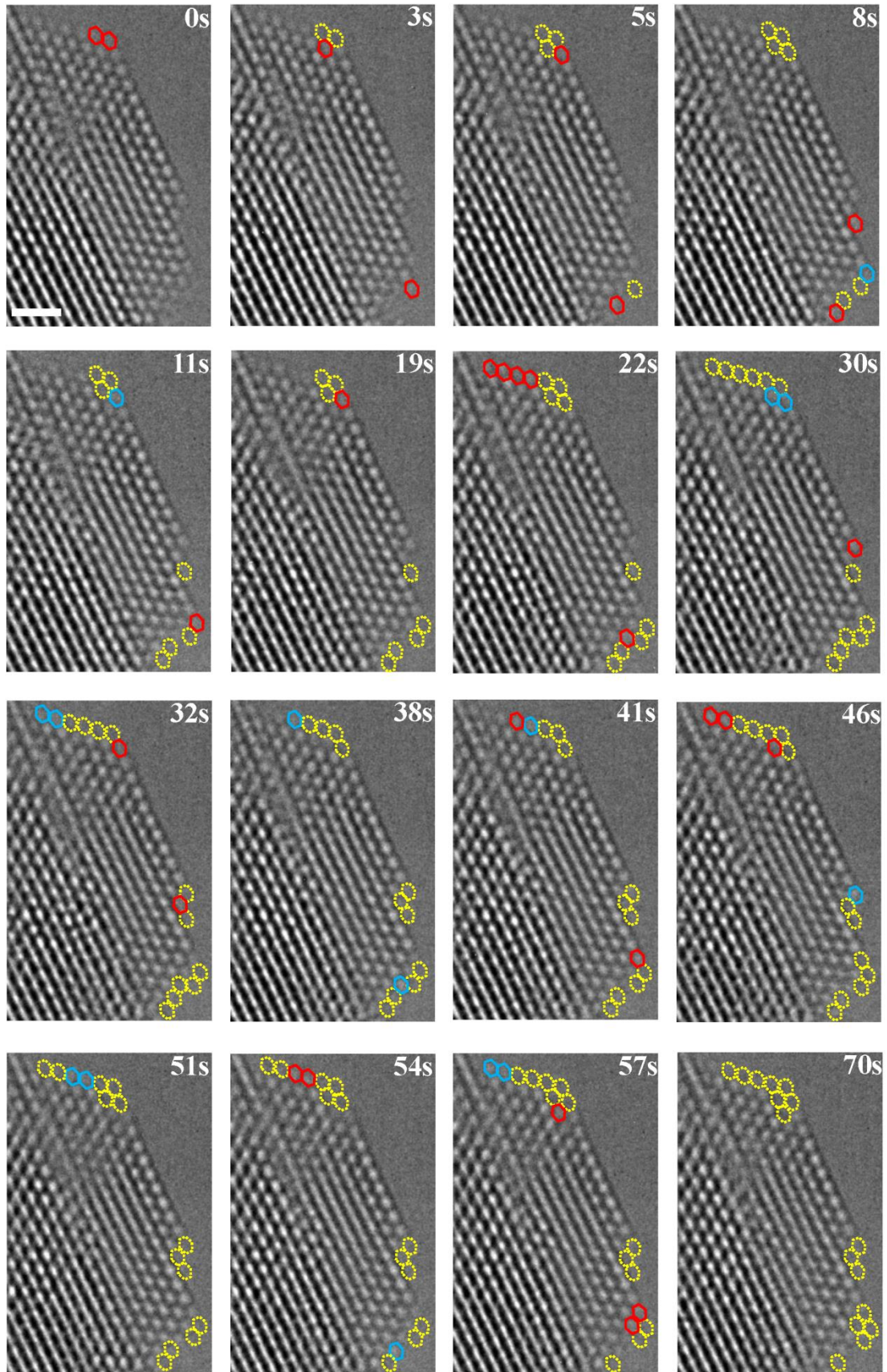
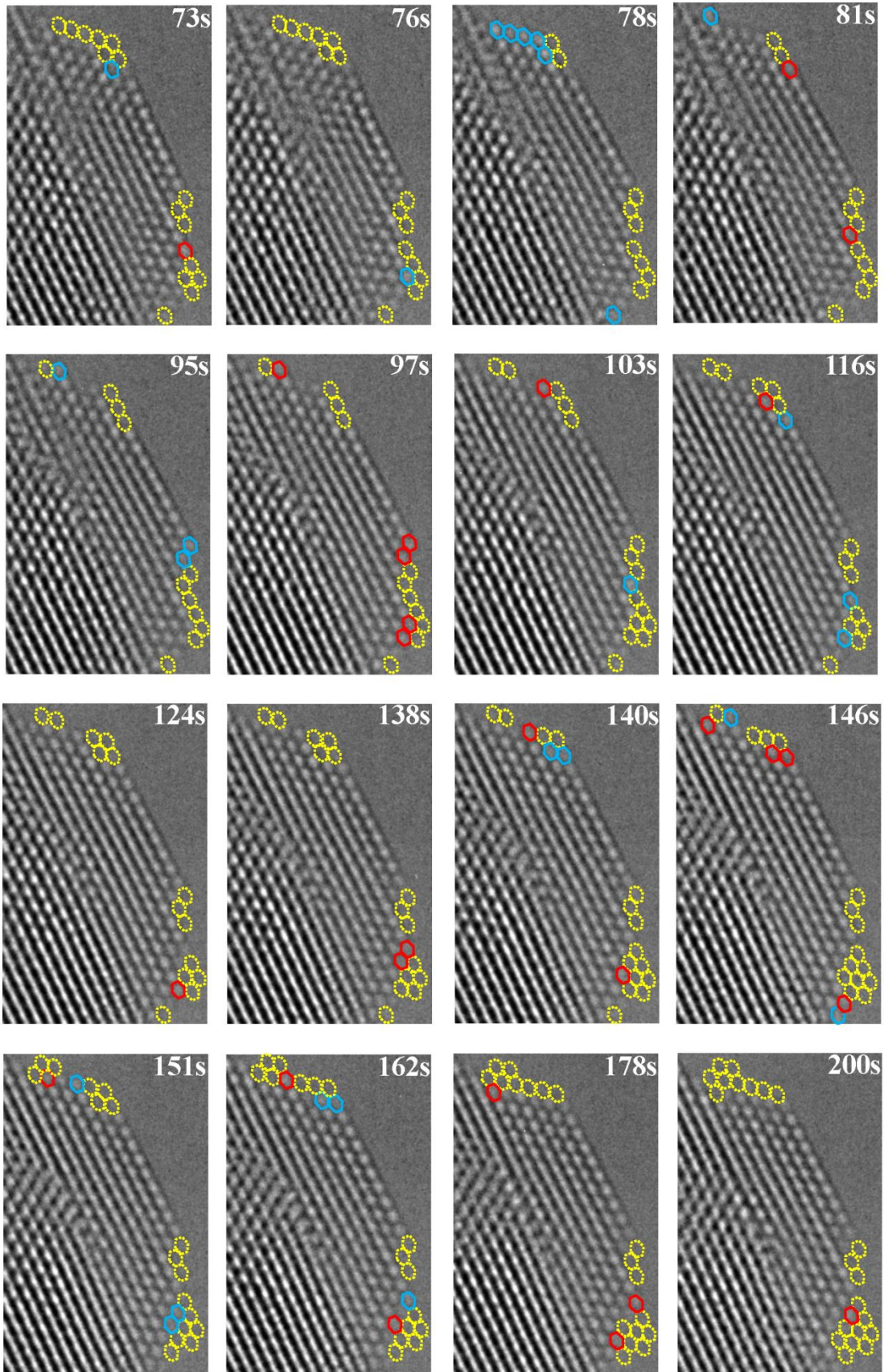
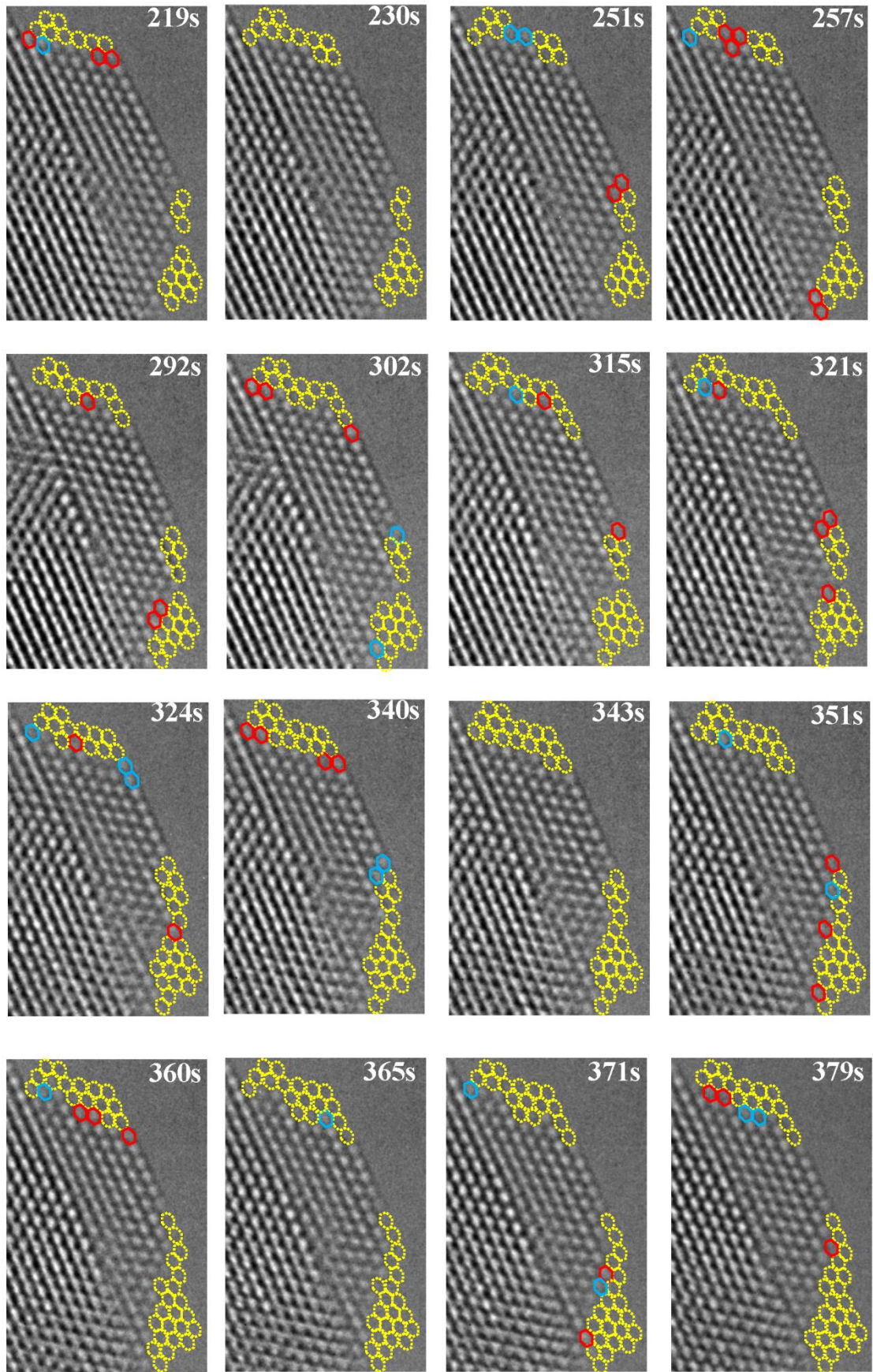
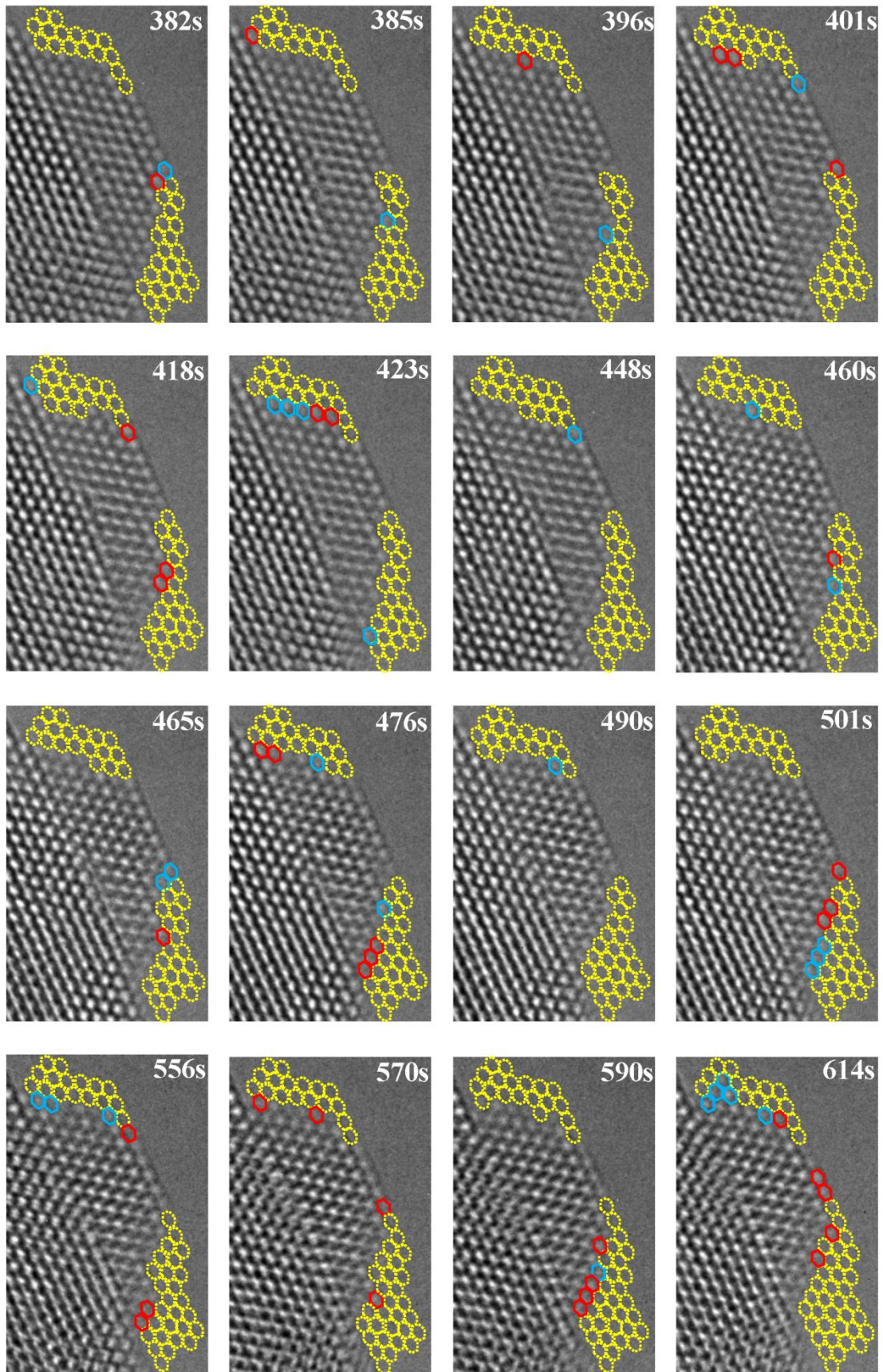


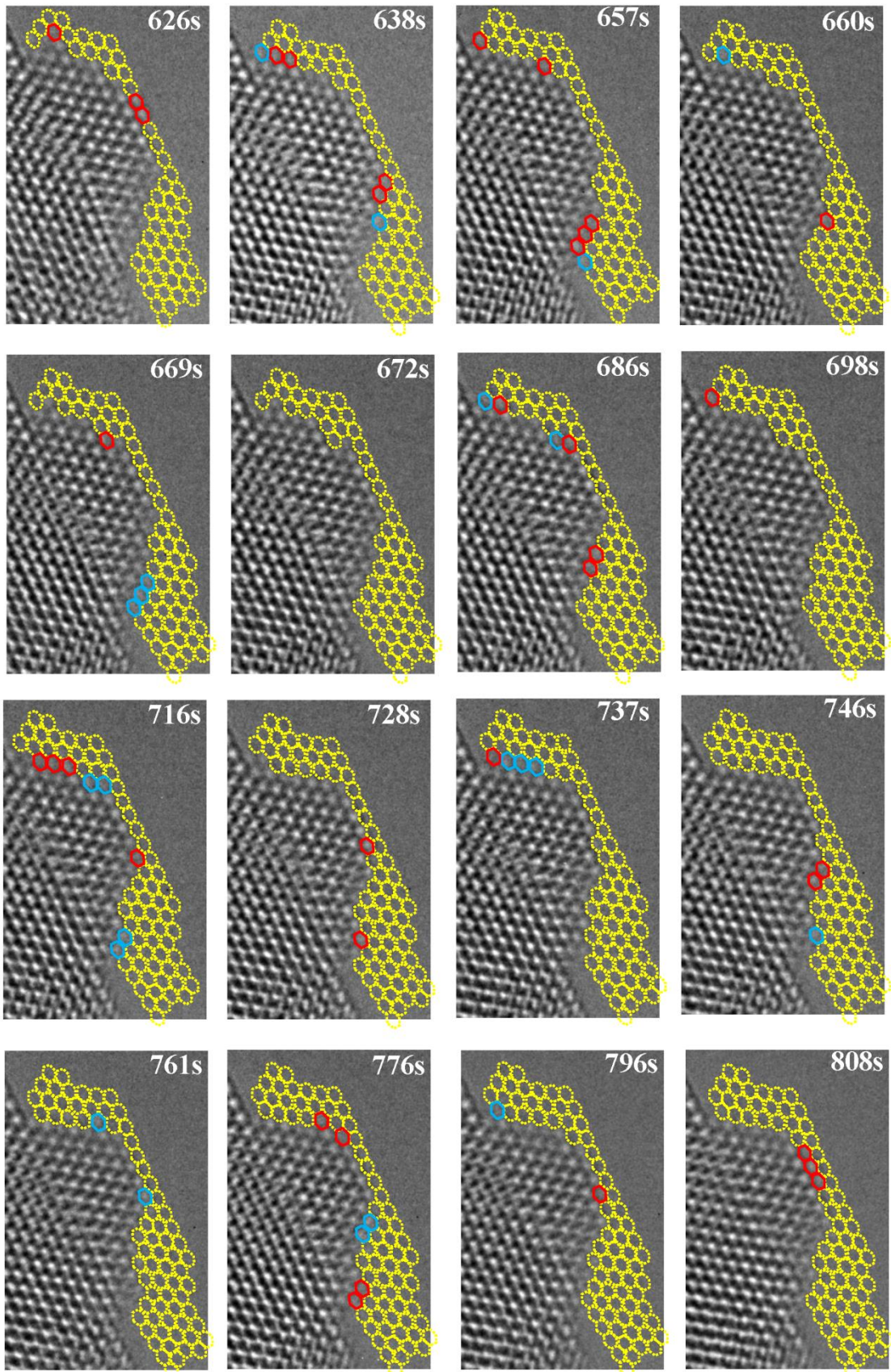
Figure S6. HRTEM image series showing the etching process of the larger CaO surface, where some of the outermost-layer atoms have been sputtered (from Video 2). The atoms with red overlays indicate that they will be sputtered in the next frame, whereas the atoms with blue overlays indicate the adatoms. The yellow overlays label the atoms that have been ejected. The frames without changes comparing with the previous frames are omitted. Scale bar is 1 nm.

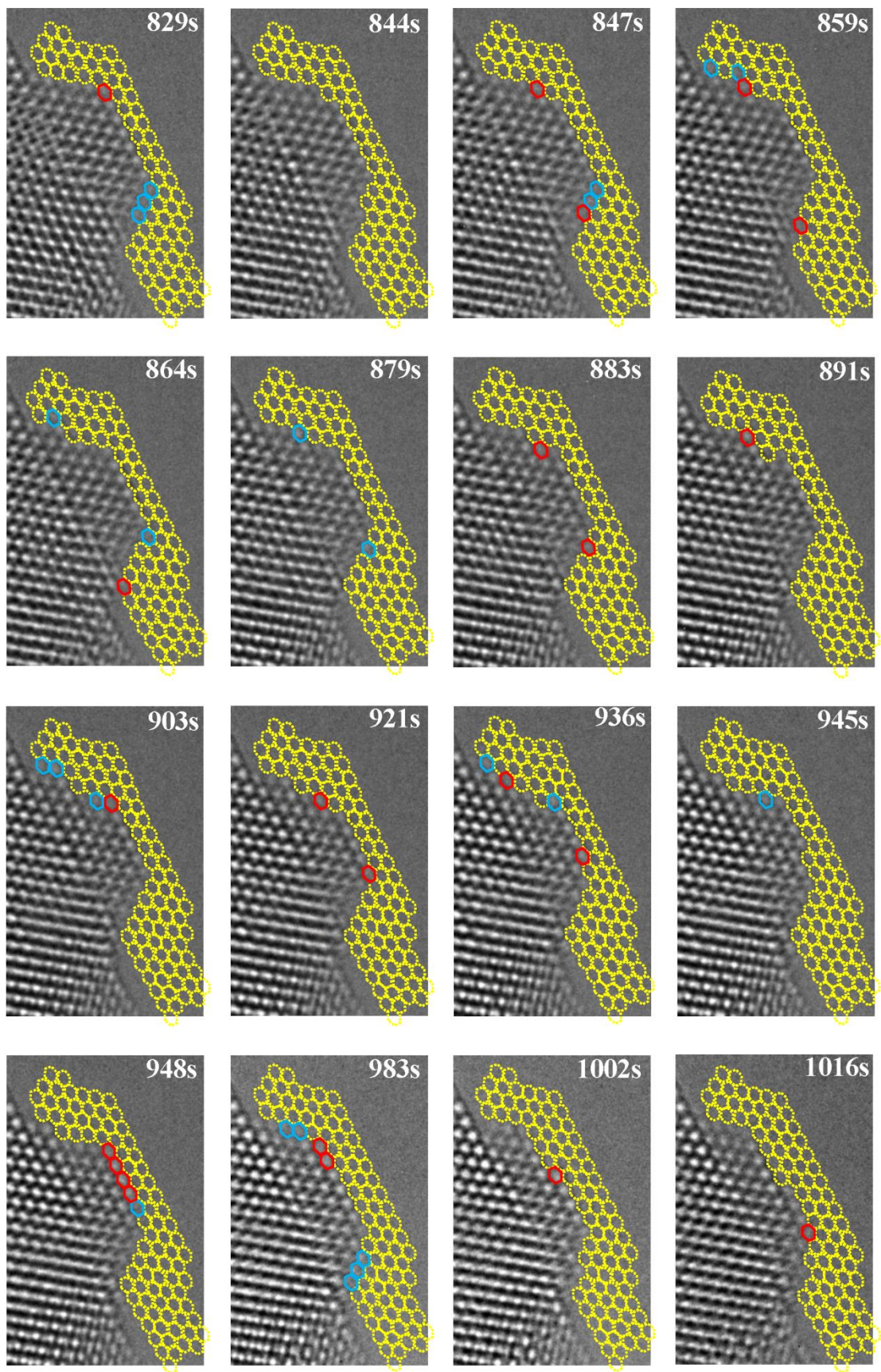


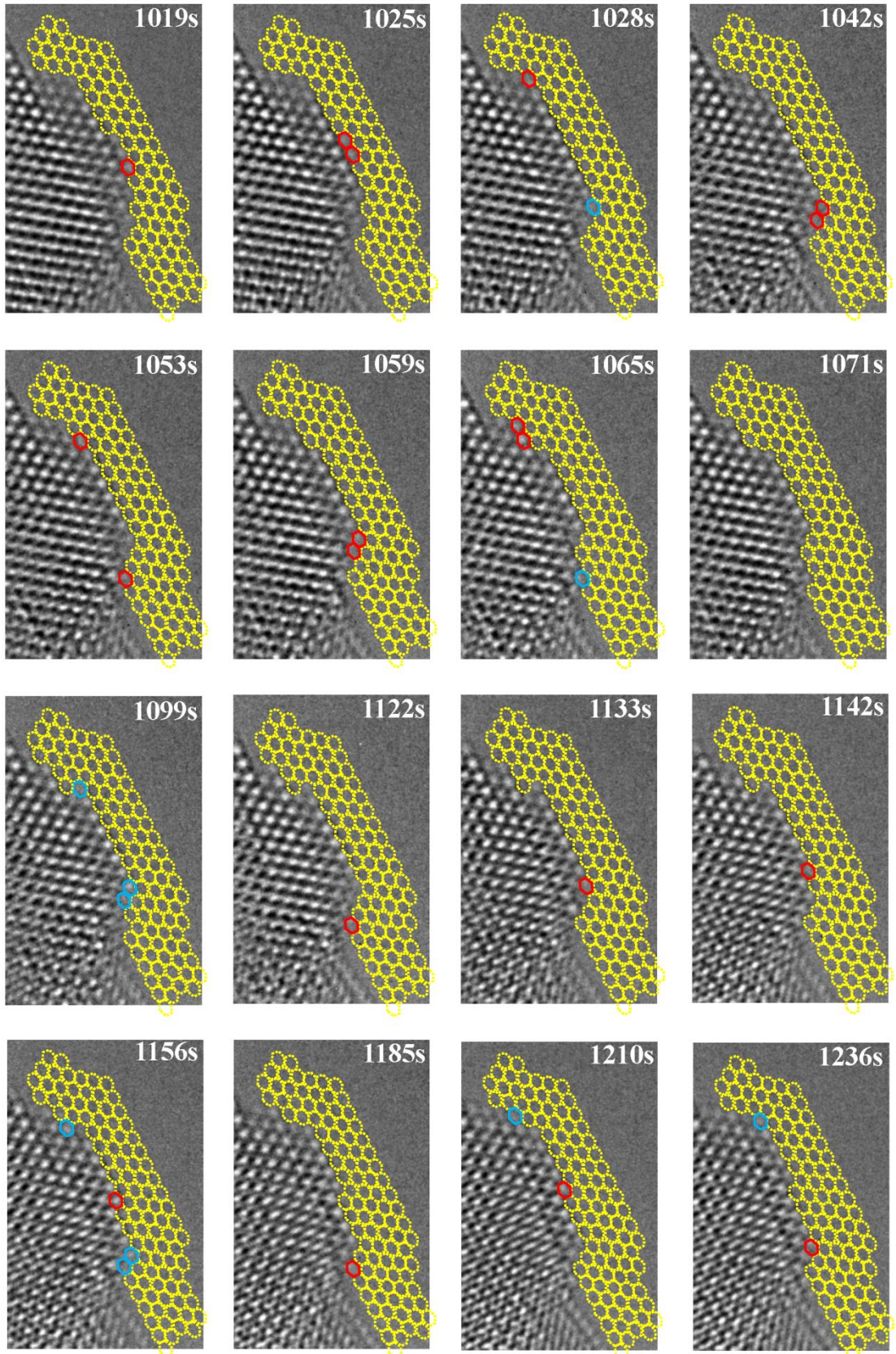


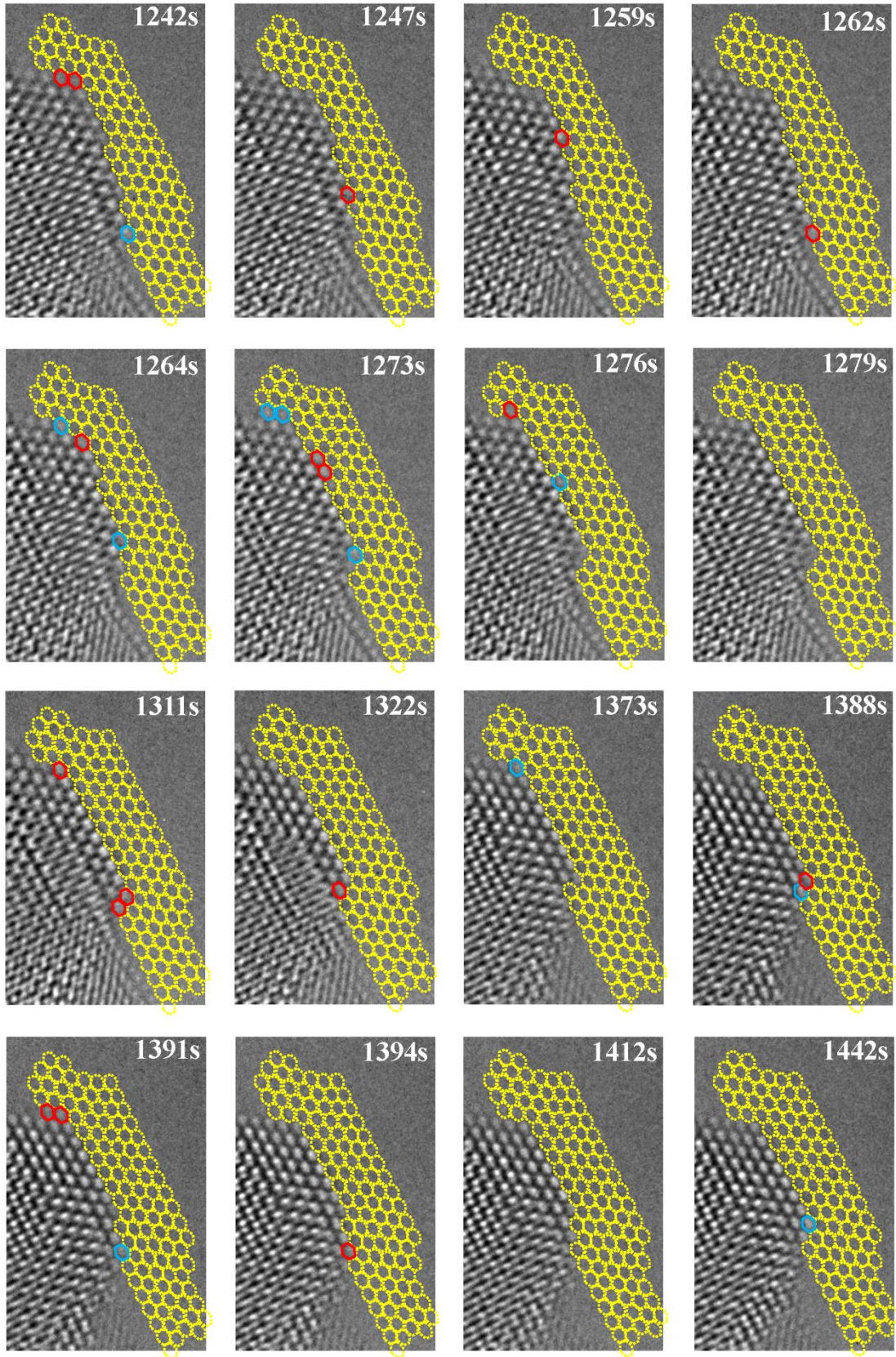












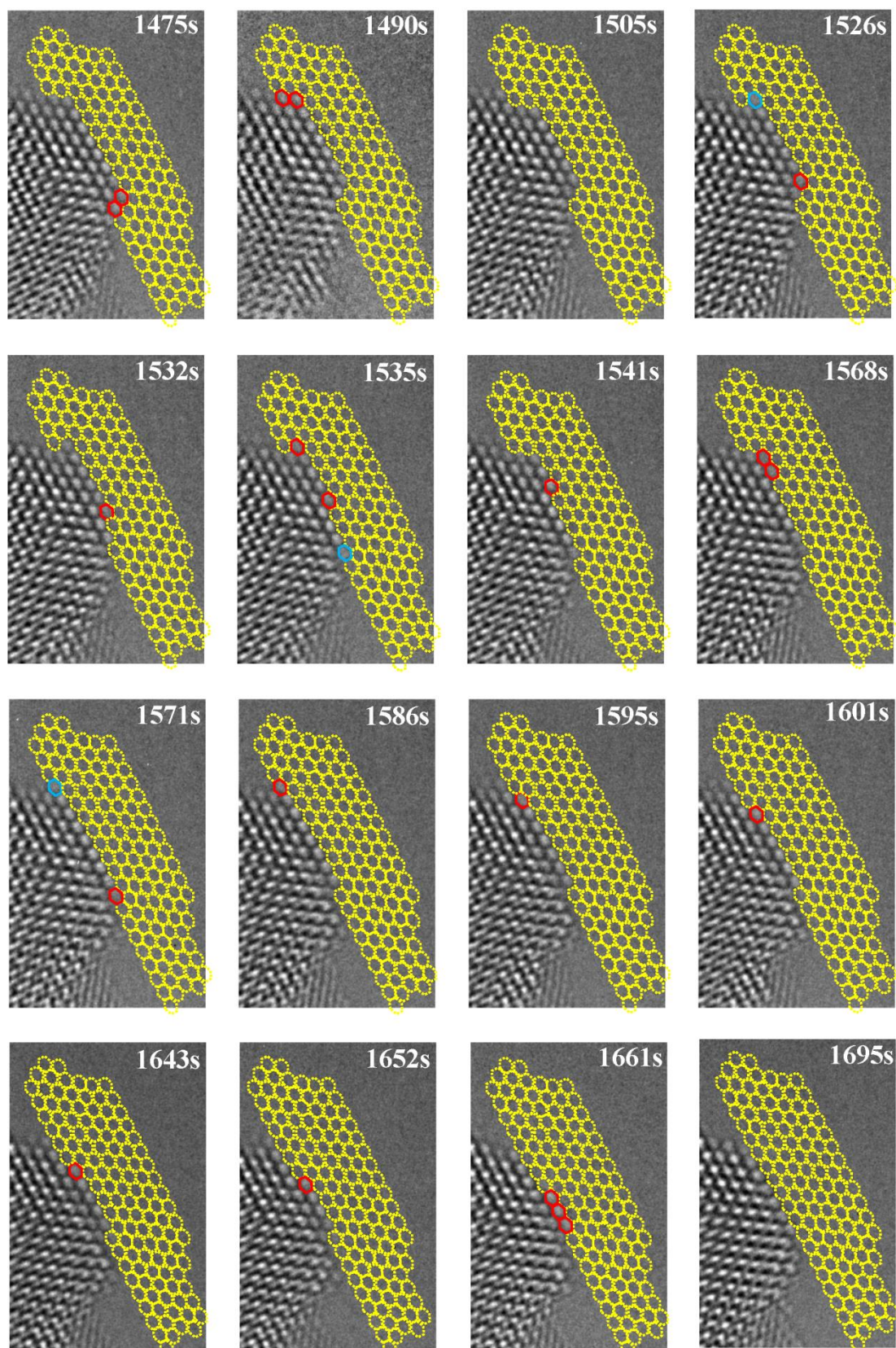
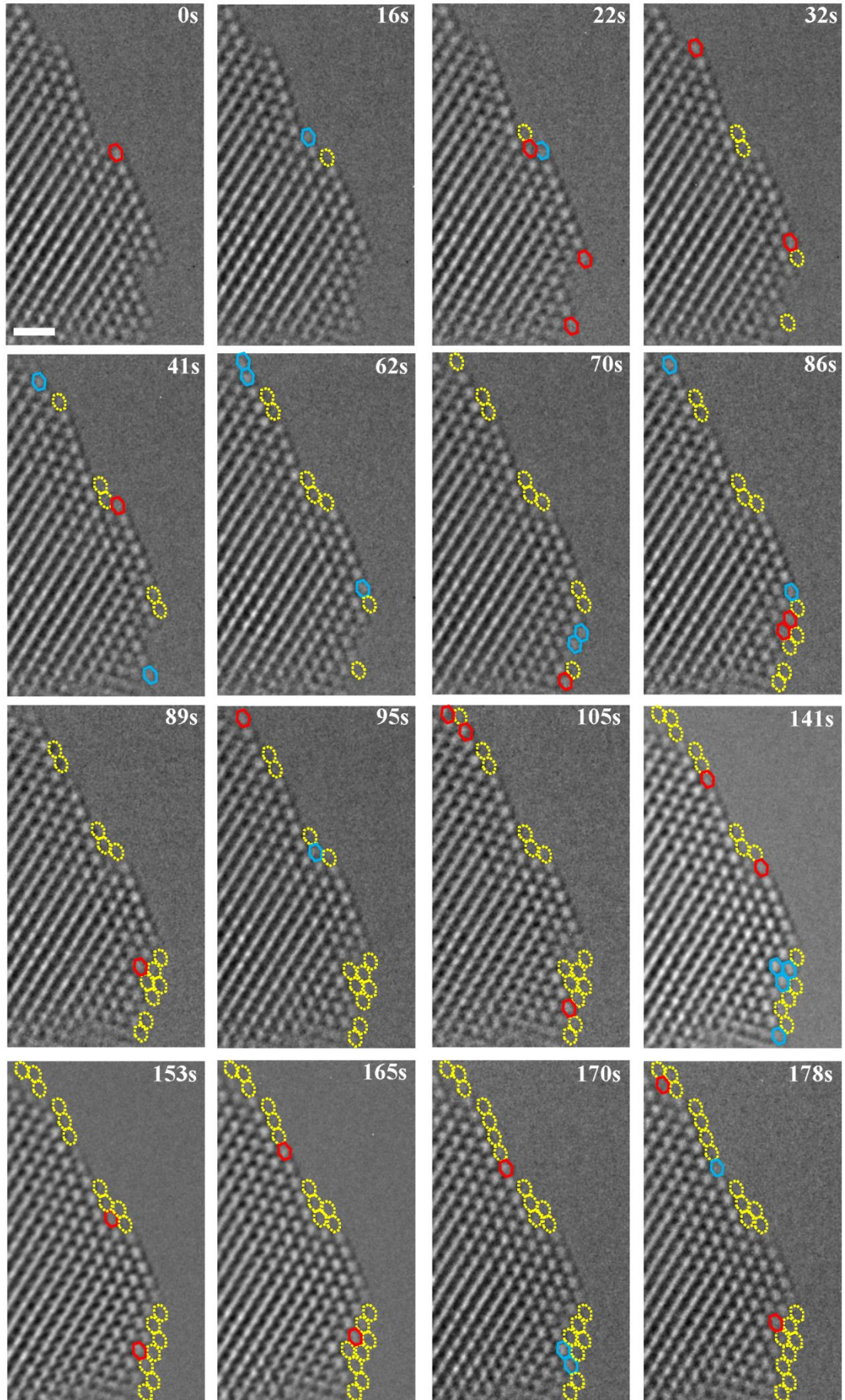
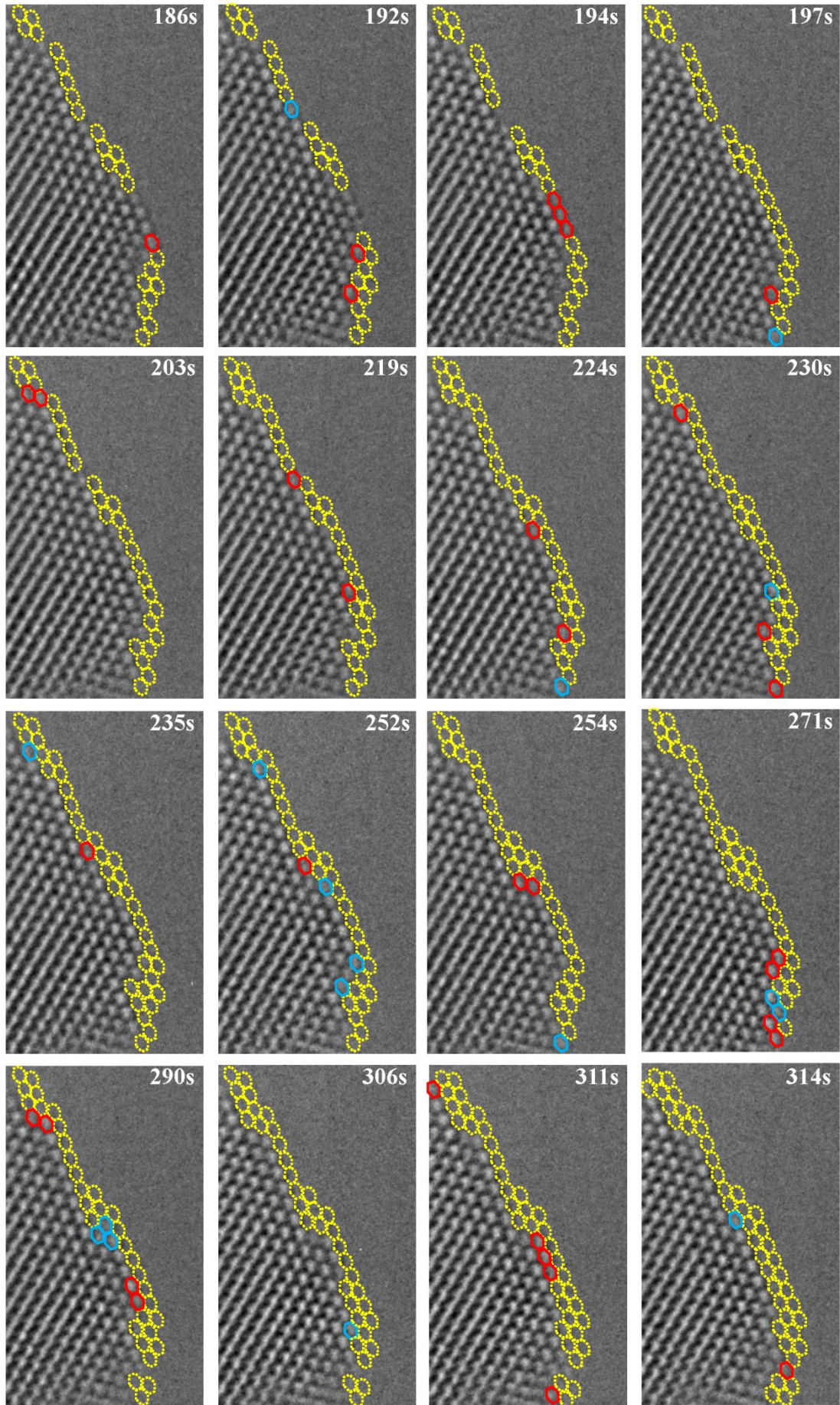
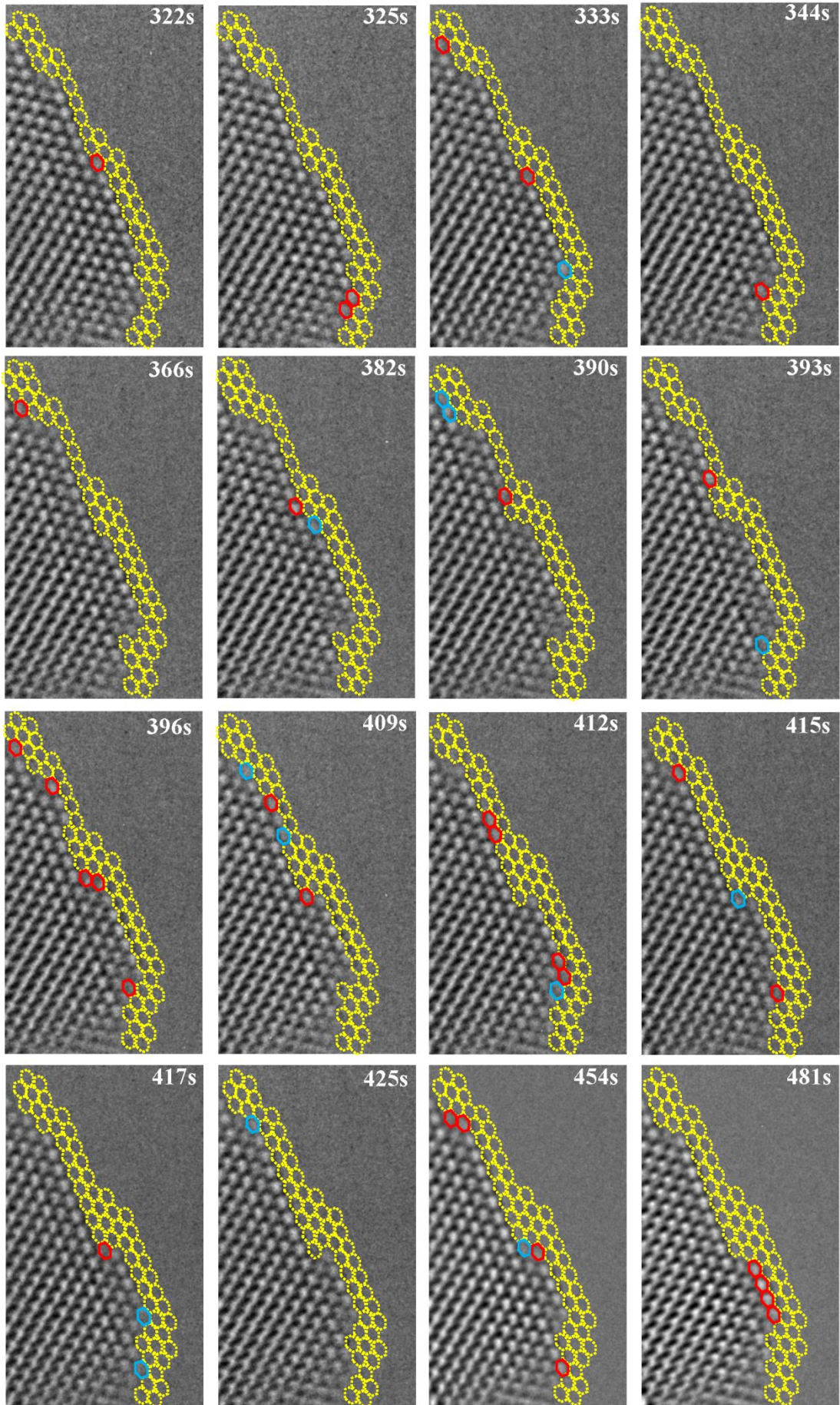


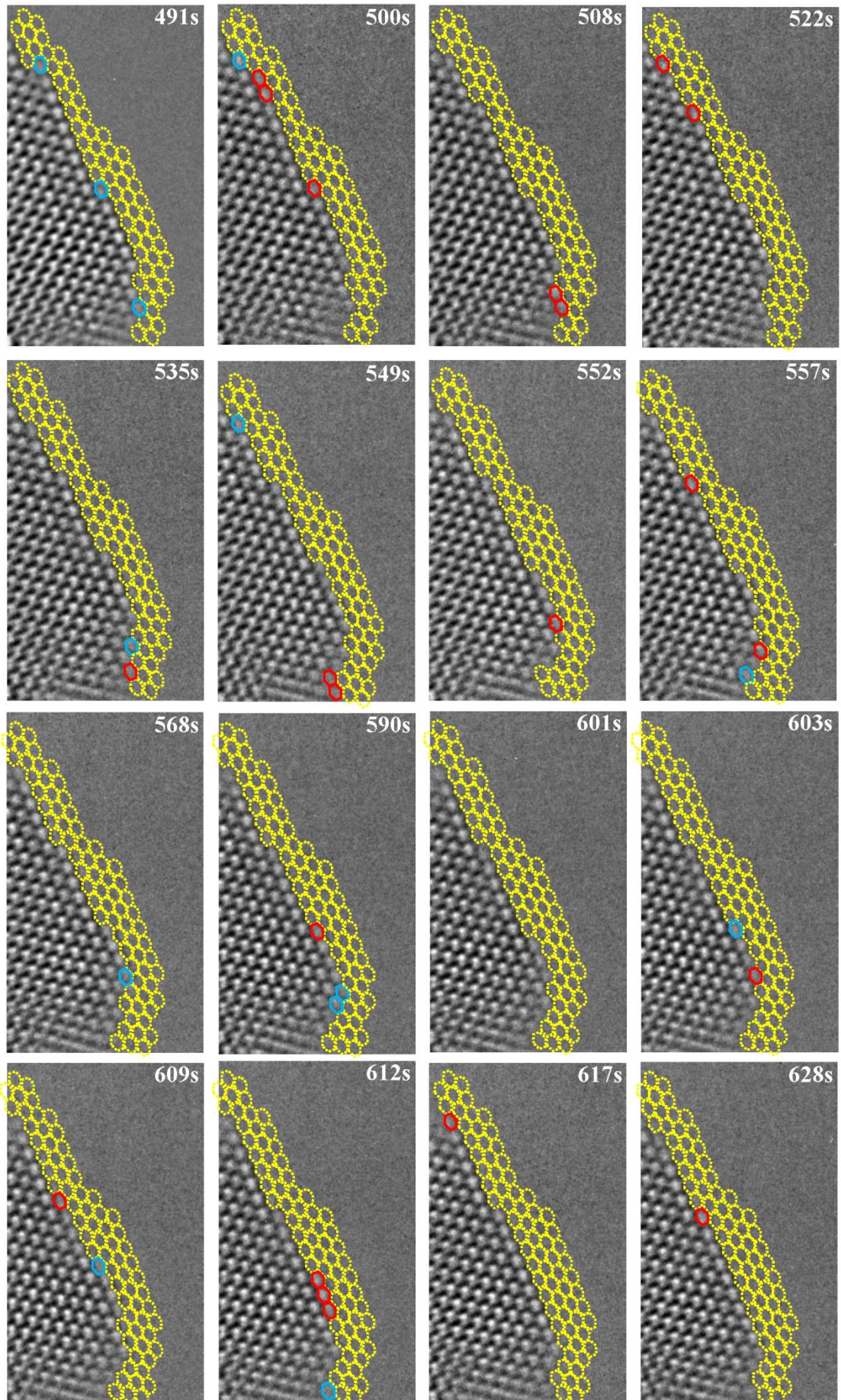
Figure S7. HRTEM image series showing the *in situ* electron beam etching process of a pyramidal island on the surface (from Video 3). The atoms with red overlays

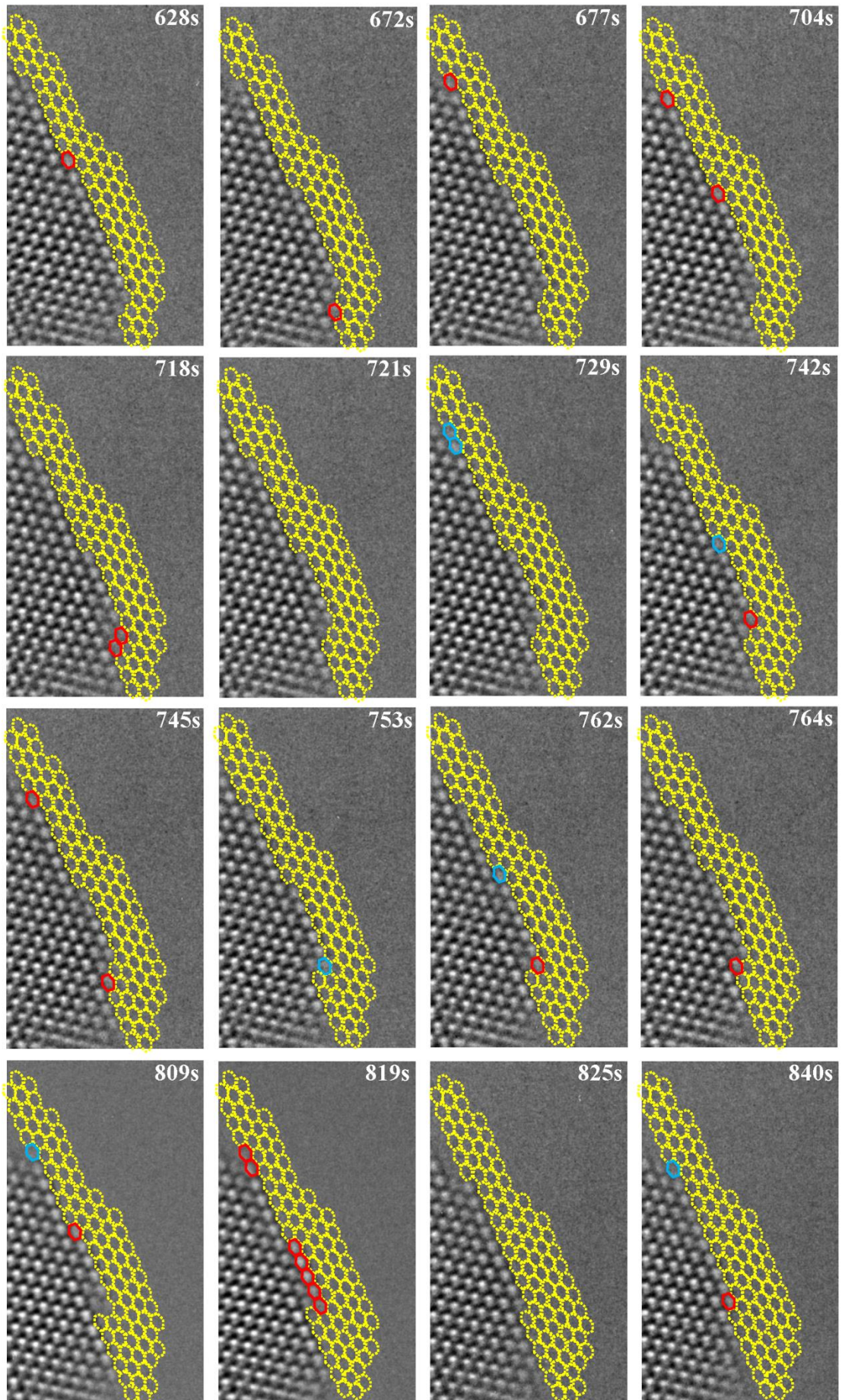
indicate that they will be sputtered in the next frame, whereas the atoms with blue overlays indicate the adatoms. The yellow overlays label the atoms that have been ejected. The frames without changes comparing with the previous frames are omitted. Scale bar is 1 nm.











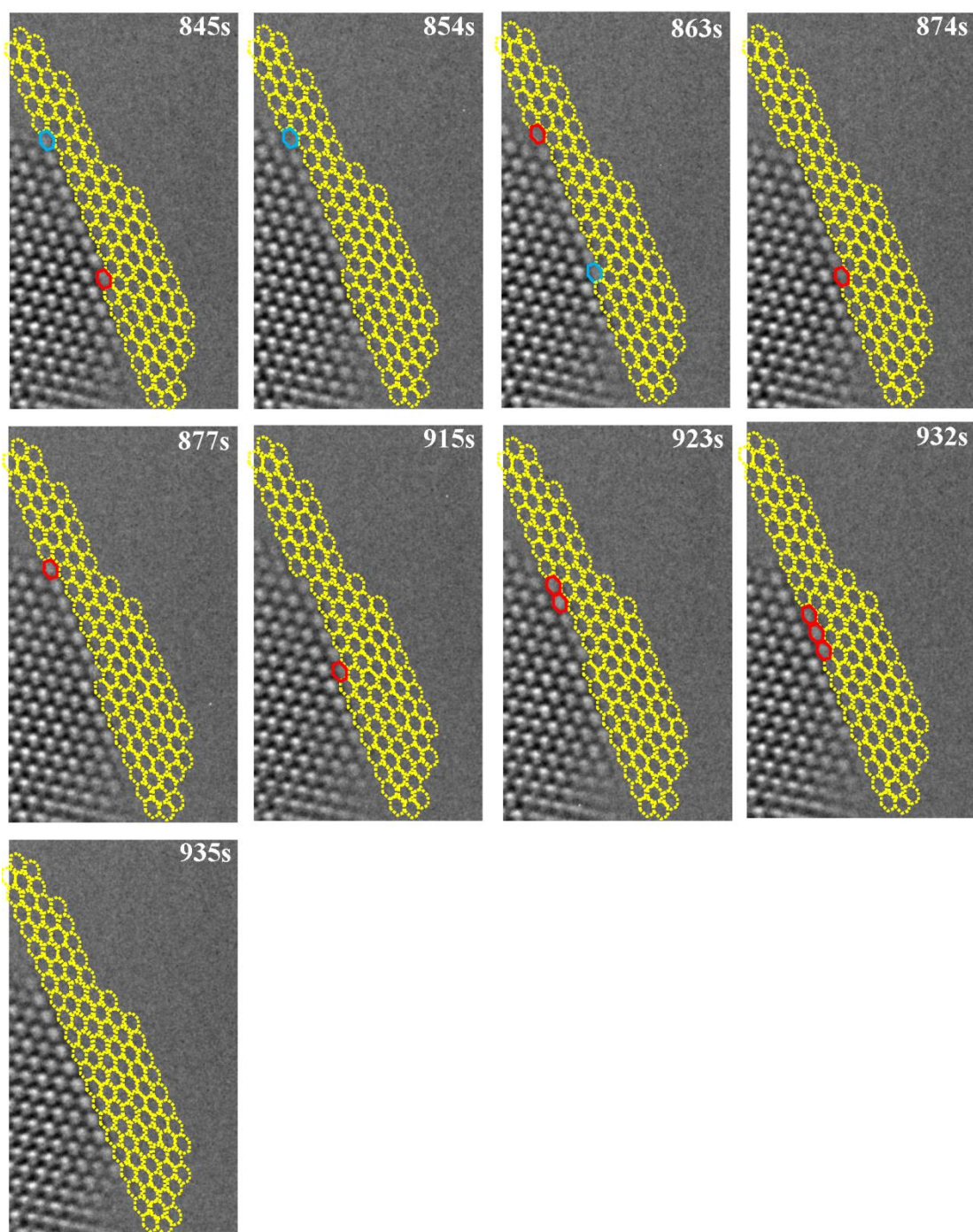
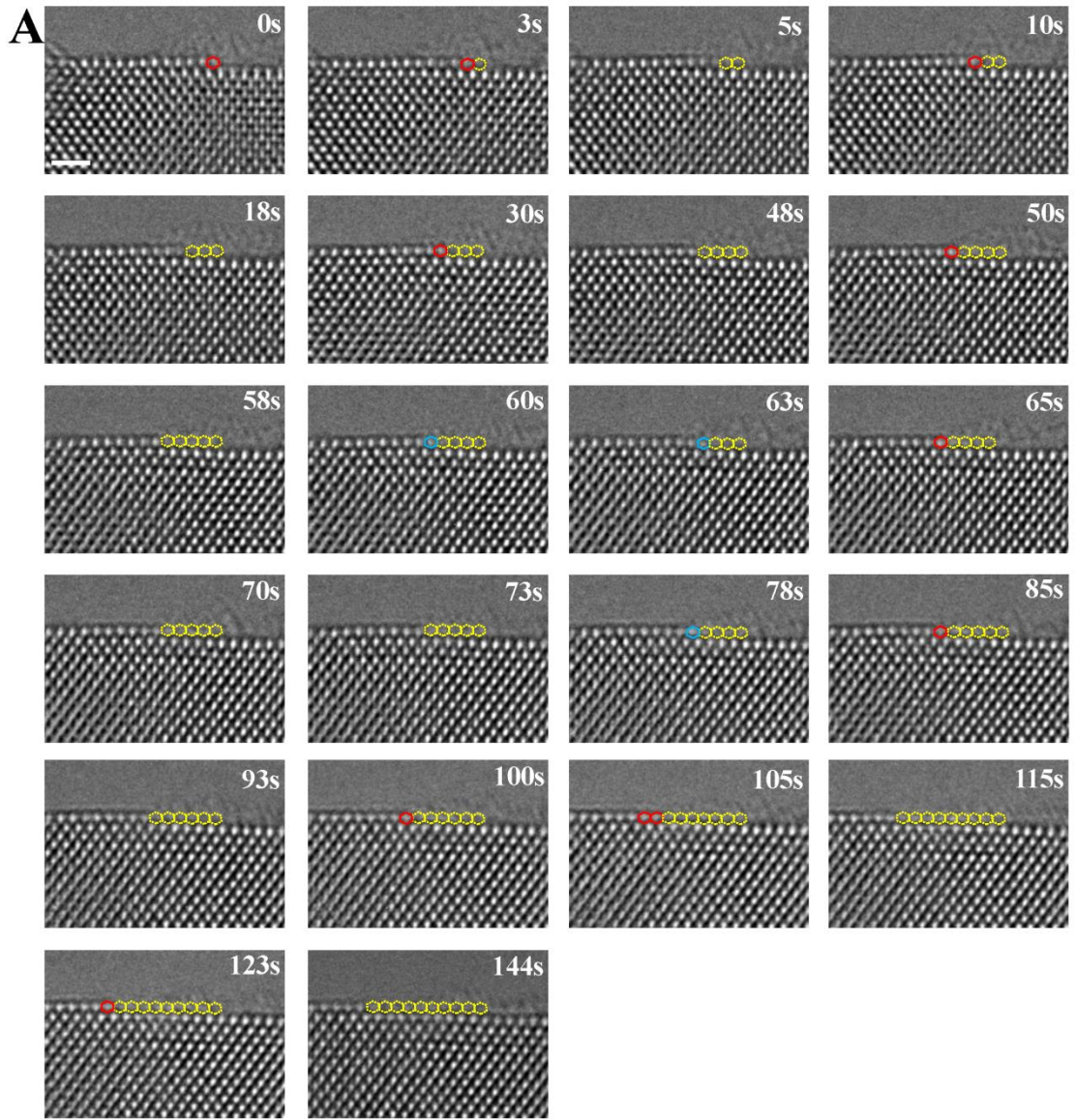


Figure S8. HRTEM image series showing the *in situ* electron beam etching process of another pyramidal CaO island (from Video 4). The atoms with red overlays indicate that they will be sputtered in the next frame, whereas the atoms with blue overlays indicate the adatoms. The yellow overlays label the atoms that have been ejected. The

frames without changes comparing with the previous frames are omitted. Scale bar is
1 nm.



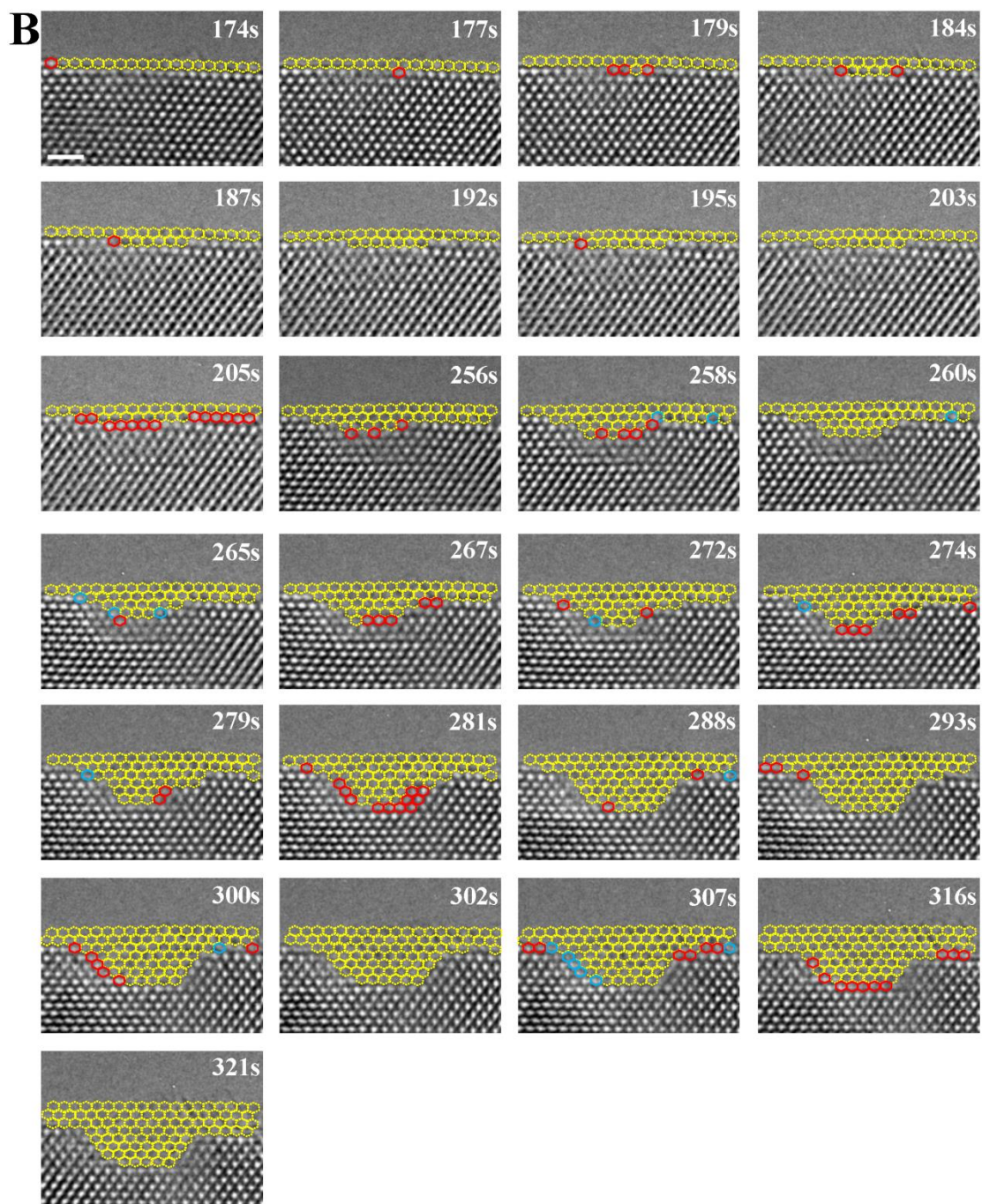


Figure S9. HRTEM image series showing the *in situ* electron beam etching process of the CaO surface with different electron beam current intensities (from Video 5): (A) $1.2 \times 10^6 \text{ A} \cdot \text{m}^{-2}$ and (B) $2 \times 10^6 \text{ A} \cdot \text{m}^{-2}$. The atoms with red overlays indicate that they will be sputtered in the next frame, whereas the atoms with blue overlays indicate the adatoms. The yellow overlays label the atoms that have been ejected. The

frames without changes comparing with the previous frames are omitted. Scale bar is 1 nm.

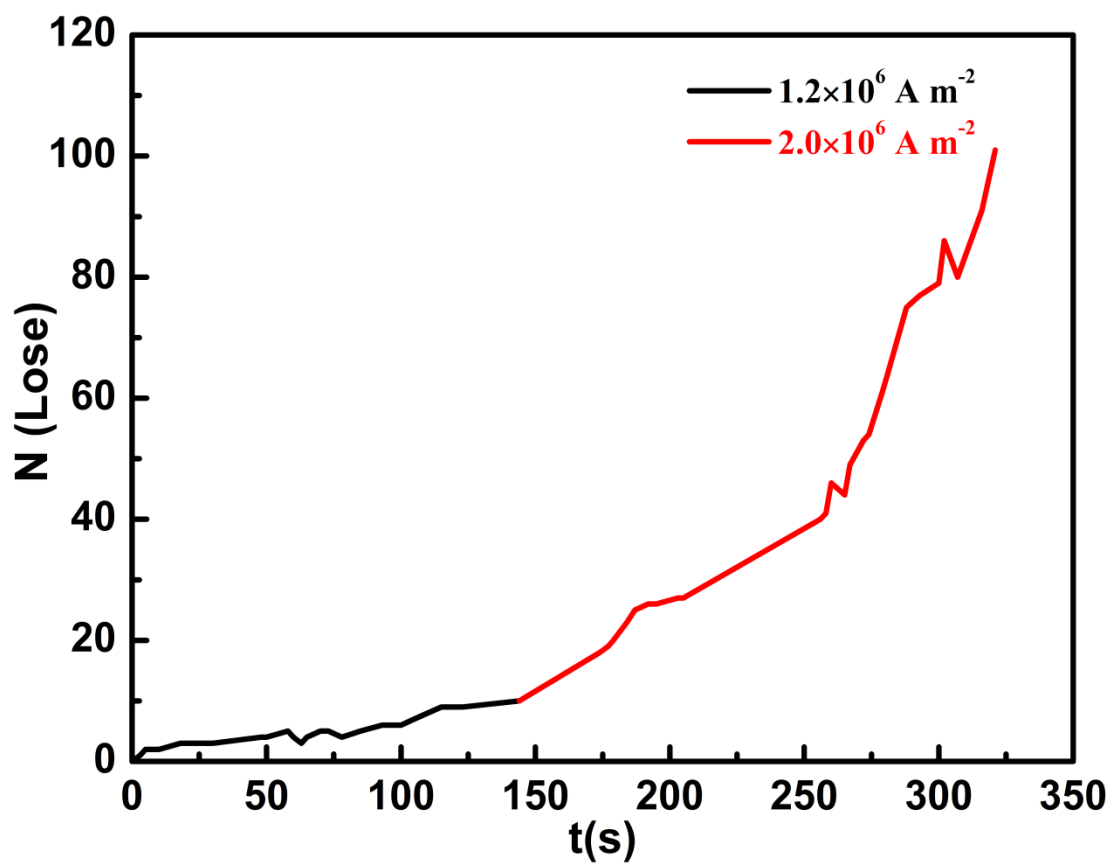


Figure S10. Etching rate under different electron beam current intensities: $1.2 \times 10^6 \text{ A} \cdot \text{m}^{-2}$ (marked with black line) and $2 \times 10^6 \text{ A} \cdot \text{m}^{-2}$ (marked with red line). The number of the lost atom columns is calculated from Figure S9 and Video 5.

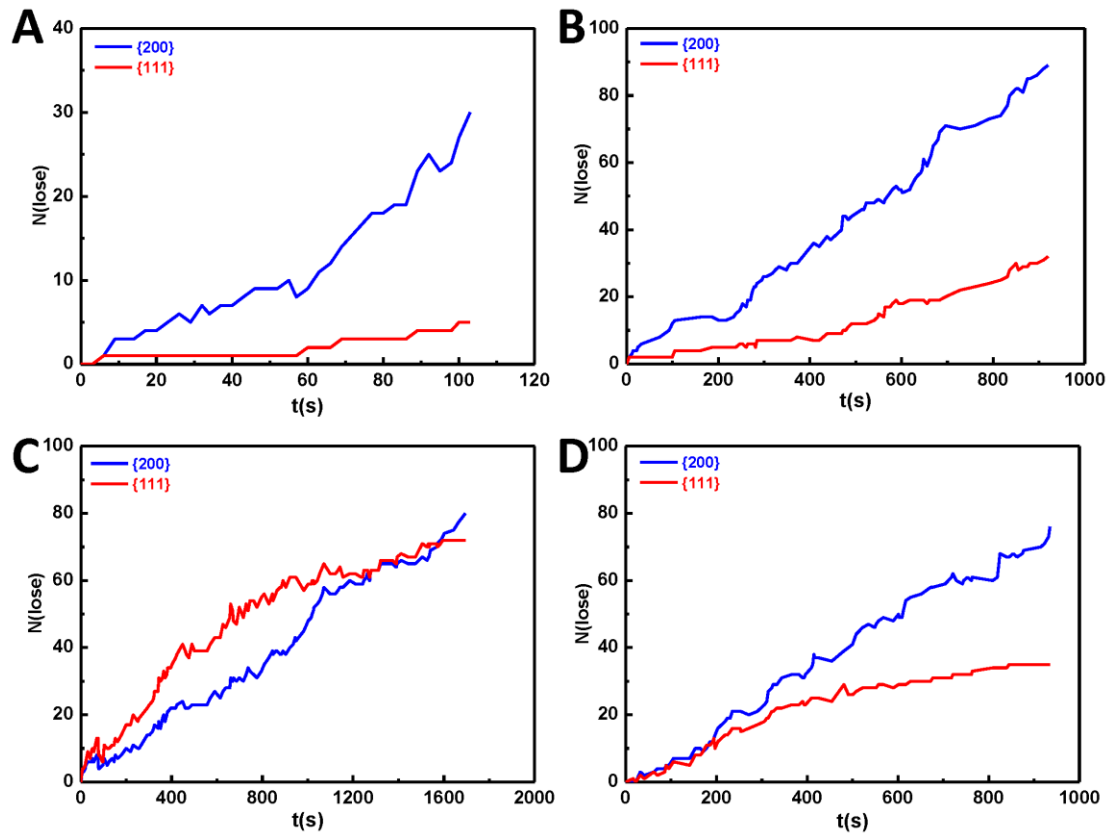


Figure S11. Etching rate of {200} and {111} facets. (A–D) Etching rate along {200} and {111} facets in the four etching processes: etching of the flat surface layers (A, B); etching of the pyramidal islands (C, D). The results in A, B, C and D are from Figures S5 (Video 1), S6 (Video 2), S7 (Video 3) and S8 (Video 4), respectively.

During the etching processes of Figure S5, S6 and S8, the etching rate of {200} facet is observably high than that of {111} facet (Figure S11A, S11B and S11D), thus the etching preferentially takes place at {200} facets.

For the estimation of the etching rate, since each atom is located on both {200} and {111} facets, there are some atoms that cannot be discriminated along which facets the etching takes place, as shown in Figure S12. We consider the etching of these atoms along the {200} and {111} facets simultaneously. And in Figure S11C, there

are a large amount of these atoms. Besides, the rim of the pyramidal island in Figure S7 has relatively long $\{111\}$ facet. As we know, the atoms at the rim have fewer neighbours, and are sputtered preferentially. Therefore, the etching rate of the two facets in Figure S11C has no significant different.

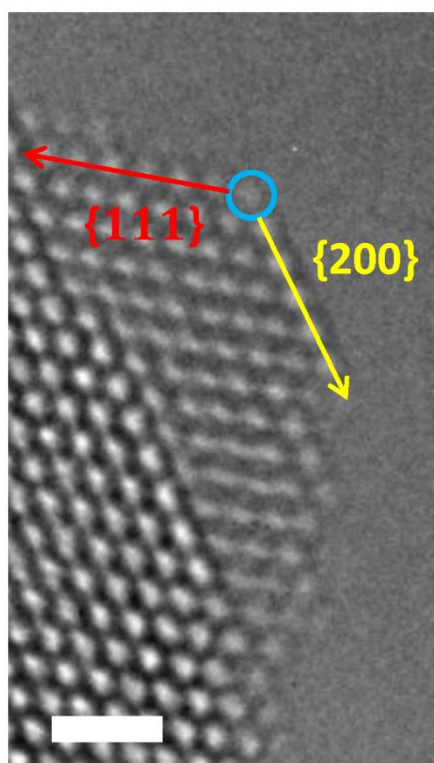


Figure S12. The atom that cannot be defined as etching along $\{200\}$ or $\{111\}$ facet.

Scale bar is 1 nm.

To sum up, at the initial etching stage of the flat surface of CaO, the sputtering is preferable at $\{200\}$ facet with a relatively high etching rate, and generates pits, where the side walls are the favourable $\{111\}$ facet. Then, it comes to the etching of pyramidal island where more $\{111\}$ facet is exposed, the etching rate of $\{111\}$ facet increases to the same level of $\{200\}$ facet.

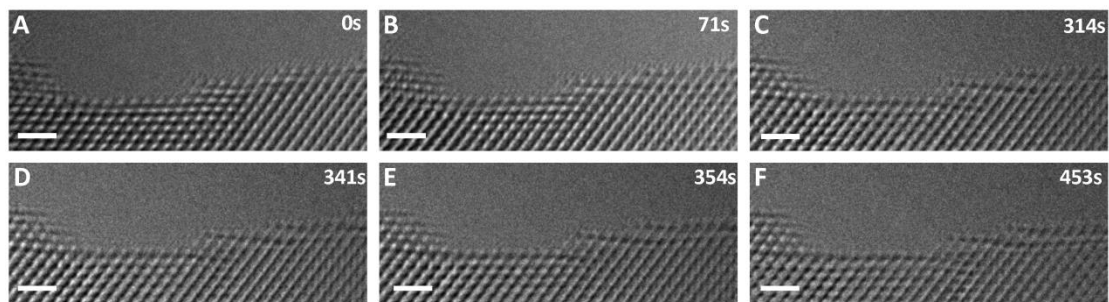


Figure S13. CaO surface under the 80 keV electron beam. (A–F) Six representative HRTEM images selected from the etching process during 453s (from Video 6). Scale bar is 1 nm.

As shown in Figure S13 and Video 6, during the irradiation of 453s, the structure was almost unchanged. 80 keV electron beam can effectively reduce the knock-on damage. Compared with 300kV, the knock-on effect of CaO at 80 kV is negligible. Thus, the 80 keV electron beam is not suitable for the etching study.

It is well known that knock-on damage increases with increasing beam energy, while damage caused by other mechanism (such as ionization) decreases.³⁻⁶ Therefore, when the beam energy is low (80 keV), ionization damage will play an important role. As shown in Figure S13, during the electron beam irradiation, the lattice gradually lost its crystal structure, which confirms that radiolysis is the dominant mechanism at 80 keV.

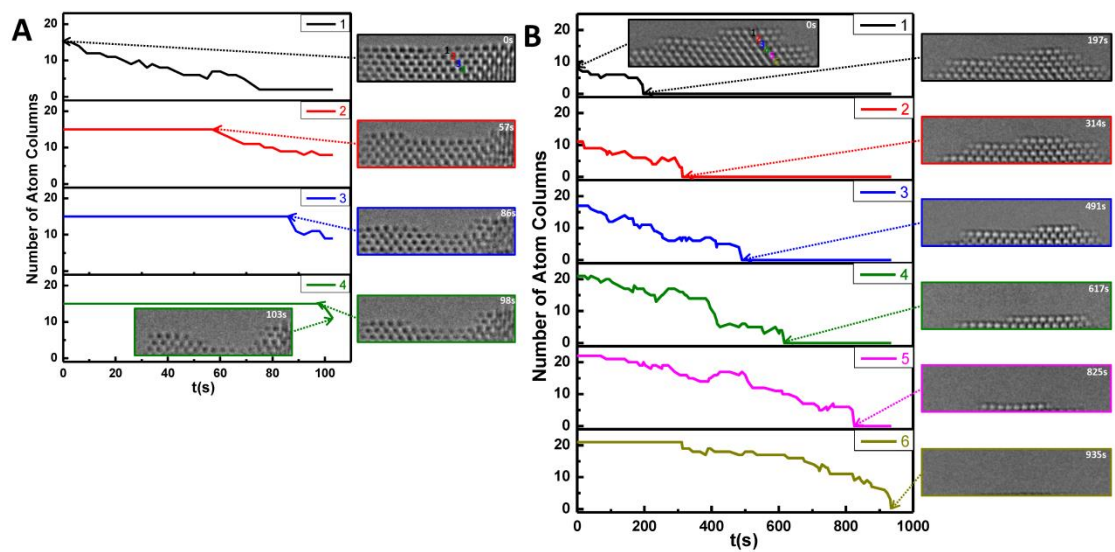


Figure S14. Time-dependent number of atom columns in each layer, shown for a flat surface (A, Video 1) and a pyramid (B, Video 4). The layers from outside to inside are numbered 1–4 (A) and 1–6 (B).

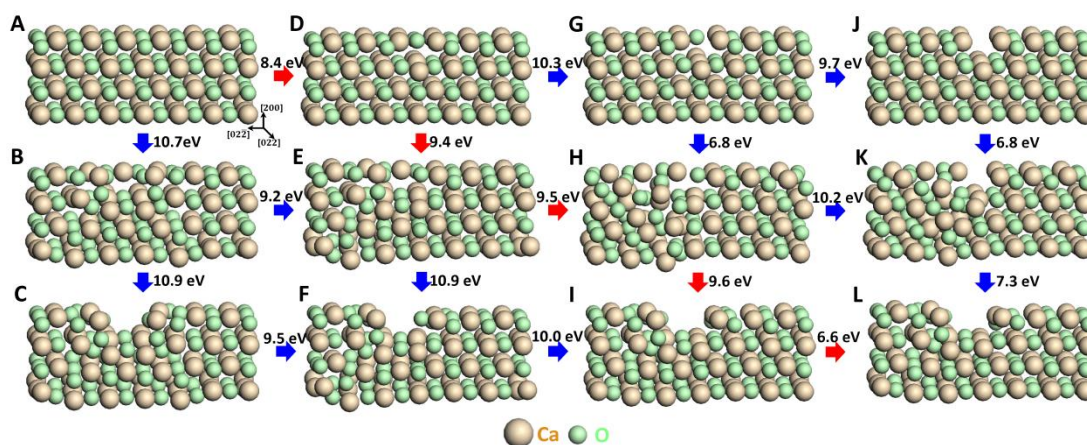


Figure S15. Schematics of the geometrical configurations of the supercell during calculation (A–L): pristine surface (A), surface with one Ca atom vacancy (B), two Ca atom vacancies (C), one O atom vacancy(D), one Ca and one O atom vacancies (E), two Ca and one O atom vacancies(F), two O atom vacancies(G), one Ca and two O atom vacancies(H), two Ca and two O atom vacancies(I), three O atom vacancies(J), one Ca and three O atom vacancies(K), two Ca and three O atom vacancies(L). The horizontal arrows indicate the sputtering of an O atom, while the vertical arrows indicate the sputtering of a Ca atom, the energy required is marked next to the arrow. The light yellow balls indicate the Ca atoms and the light green balls indicate the O atoms.

Notably, the geometrical configurations in Figure S15 are obtained after full relaxation, in which some atoms are not in the initial positions and may be blocked by other atoms.

To simulate the case of removing a single Ca or O atom away from the edge of the CaO surface, all the calculations were carried out for the supercell configurations

represented in Figure S15. Figure S15A shows the pristine CaO surface. When a Ca atom is removed away from its edge site, the geometrical configuration of system is reconstructed, as shown in Figure S15B. Then, dislodging an O atom adjacent to the Ca atom vacancy from configuration B, the structure of system turns to the configuration showed in Figure S15E. Or, another Ca atom along the same atom arrays in configuration B is sputtered, the geometrical configuration is shown in Figure S15C. The rest circumstances can be done in the same manner.

To characterize the binding capacity of Ca atom from configuration B to A, we calculated the binding energy E_b , which is defined as $E_b = E[\text{Ca}] + E[\text{B}] - E[\text{A}]$, where $E[\text{Ca}]$, $E[\text{B}]$, and $E[\text{A}]$ represent the energies of isolated Ca atom, configuration B, and configuration A, respectively. In Figure S15A-L, we summarized the binding energies for different cases adjacent to the arrows.

It is known that TEM images are actually 2D projections of a 3D sample and the spots we see represent columns of atoms. Thus, *in situ* HRTEM observation could only provide evidence for the etching of atom columns. Through calculation, we can achieve more detailed etching process atom by atom. As shown in Figure S15, the etching process is carried out along the red arrows in the order of O–Ca–O–Ca–O.

For the equation (1) in the main text

$$T = \frac{2E_{min}(E_{min} + 2m_e c^2)}{Mc^2}$$

E_{min} is the root of the quadratic equation.

$$E_{min} = -m_e c^2 \pm \sqrt{(m_e c^2)^2 + (Mc^2/2)T}$$

As the value of E_{min} is positive, the E_{min} is calculated by

$$E_{min} = \sqrt{(m_e c^2)^2 + (Mc^2/2)T} - m_e c^2$$

where T is the binding energy, the maximum binding energy of Ca and O during the calculation is $T_{Ca}=10.9$ eV and $T_O= 10.3$ eV, $m_e=9.1 \times 10^{-31}$ kg, $c=3 \times 10^8$ m/s, $M_{Ca}=40 \times 1.67 \times 10^{-27}$ kg, $M_O=16 \times 1.67 \times 10^{-27}$ kg. Thus, E_{min} of Ca and O atom is 171 keV and 71 keV, respectively.

Video 1: *In situ* electron beam etching process of the CaO surface under 300 kV electron irradiation.

Video 2: *In situ* electron beam etching process of the larger CaO surface under 300 kV electron irradiation, where some of the outermost-layer atoms have been sputtered.

Video 3: *In situ* electron beam etching process of a pyramidal CaO island on the surface under 300 kV electron irradiation.

Video 4: *In situ* electron beam etching process of another pyramidal CaO island under 300 kV electron irradiation.

Video 5: *In situ* electron beam etching process of the CaO surface with different electron beam current intensities: $1.2 \times 10^6 \text{ A} \cdot \text{m}^{-2}$ and $2 \times 10^6 \text{ A} \cdot \text{m}^{-2}$ under 300 kV electron irradiation.

Video 6: *In situ* electron beam etching process of the CaO surface under 80 kV electron irradiation.

REFERENCES

1. Golla-Schindler, U., et al. *Microsc. Microanal.* **2014**, 20, 715-722.
2. Hofer, F.; Golob, P. *Ultramicroscopy* **1987**, 21, 379-383.
3. Williams, D. B.; Carter, C. B., *Transmission Electron Microscopy*. 2nd ed.; Springer: New York, 2009.
4. Kim, H. M., et al. *Nanotechnology* **2011**, 22, 275303.
5. Ugurlu, O., et al. *Phys. Rev. B* **2011**, 83, 113408.
6. Csencsits, R.; Gronsky, R. *Ultramicroscopy* **1987**, 23, 421-431.